AD-A128 397 SYSTEMS AND APPLIED SCIENCES CORP RIVERDALE MD F/G 4/2
SPECTRAL CHARACTERISTICS OF THE GLOBAL MOISTURE DISTRIBUTION AN--ETC(U)
JUL 82 D C NORQUIST, C JOHNSON F19628-82-C-0023
UNCLASSIFIED SCIENTIFIC-1 AFGL-TR-82-0190 NL

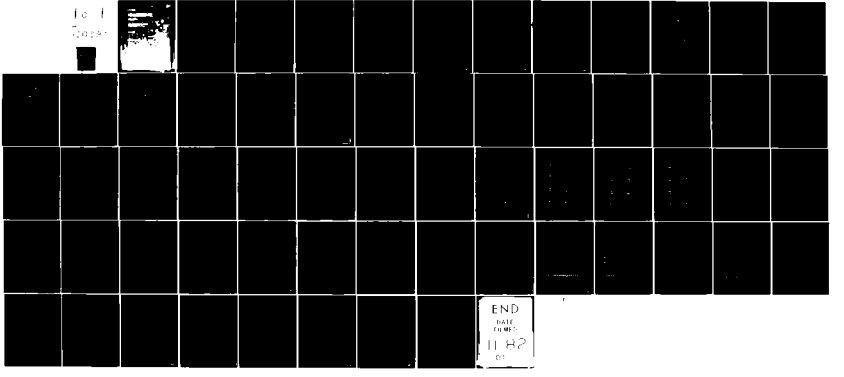

UNCLASSIFIED

SECURITY CLASSIFICATION OF THIS PAGE (When Data Entered)

REPORT DOCUMENTATION PAGE		READ INSTRUCTIONS BEFORE COMPLETING FORM
1. REPORT NUMBER AFGL-TR-82-0190	2. GOVT ACCESSION NO. AD-A120397	3. RECIPIENT'S CATALOG NUMBER
4. TITLE (and Subtitle) SPECTRAL CHARACTERISTICS OF THE GLOBAL MOISTURE DISTRIBUTION AND THEIR IMPORTANCE IN OBJECTIVE ANALYSIS OF MOISTURE FOR NWP MODELS		5. TYPE OF REPORT & PERIOD COVERED Scientific Report No. 1 6. PERFORMING ORG. REPORT NUMBER
7. AUTHOR(s) Donald C. Norquist Chris Johnson		8. CONTRACT OR GRANT NUMBER(s) F19628-82-C-0023
9. PERFORMING ORGANIZATION NAME AND ADDRESS Systems and Applied Sciences Corporation 6811 Kenilworth Avenue Riverdale, MD 20737		10. PROGRAM ELEMENT, PROJECT, TASK AREA & WORK UNIT NUMBERS 61102F 667000AC
11. CONTROLLING OFFICE NAME AND ADDRESS Air Force Geophysics Laboratory Hanscom AFB, MA 01731 Manager/Charles Burger/LYT		12. REPORT DATE July 14, 1982 13. NUMBER OF PAGES 61
14. MONITORING AGENCY NAME & ADDRESS(if different from Controlling Office)		15. SECURITY CLASS. (of this report) UNCLASSIFIED 15a. DECLASSIFICATION/DOWNGRADING SCHEDULE

16. DISTRIBUTION STATEMENT (of this Report)

Approved for public release; distribution unlimited.

17. DISTRIBUTION STATEMENT (of the abstract entered in Block 20, if different from Report)

18. SUPPLEMENTARY NOTES

19. KEY WORDS (Continue on reverse side if necessary and identify by block number)

SPECIFIC HUMIDITY	OBJECTIVE ANALYSIS
HARMONIC ANALYSIS	RHOMBOIDAL TRUNCATION
MODEL INITIAL CONDITIONS	ZONAL HARMONIC POWER
MOISTURE POWER SPECTRUM	SPHERICAL HARMONIC POWER

20. ABSTRACT (Continue on reverse side if necessary and identify by block number)

Using data sets of observations of atmospheric variables on a global scale, the spectral distribution of atmospheric moisture is compared with that of wind and mass fields. Results show that, spectrally, the wind field has more of its power in higher wave numbers, and temperature and geopotential height have more power in lower wave numbers, than does moisture. Moisture has a shift in its power toward higher wave number with altitude, contrasting with a greater concentration of power in low wave numbers with altitude for geopotential. A baseline against which objective analysis methods for the

DD FORM 1 JAN 73 1473 EDITION OF 1 NOV 65 IS OBSOLETE

UNCLASSIFIED

SECURITY CLASSIFICATION OF THIS PAGE (When Data Entered)

respective variables may be tested is established, to determine how accurately each method represents the observed field. It is concluded on the basis of the unique characteristics of the moisture spectrum that special attention should be given to the design of a moisture analysis method.

Accession For	
NTIS GRA&I	☒
DTIC TAB	☐
Unannounced	☐
Justification	
By	
Distribution/	
Availability Codes	
Dist	Avail and/or Special
A	

TABLE OF CONTENTS

I. Introduction

A weakness of many operational numerical weather prediction (NWP) models has been the forecast accuracy of the distribution and intensity of precipitation, and the accompanying forecast fields of atmospheric moisture. Most models use the equation for the conservation of mass of water vapor represented by some form of absolute humidity, along with source and sink parameterizations of evaporation-condensation processes such as large-scale and convective scale precipitation. Certainly, the parameterizations may inadequately simulate the corresponding atmospheric phenomena, but improper specification of the initial distribution of atmospheric moisture could also contribute significantly to forecast errors. Many presently used moisture analysis methods treat moisture in much the same manner as the other mass fields, without any special attention to any similarities or differences that may exist between moisture and other mass field distributions. This report describes a study which attempts to determine the general characteristics of the global moisture distribution and to compare the features of their spectral composition to those of the mass and motion field parameters. This comparison will allow for the more realistic design of a moisture analysis method in which the similarities and differences of moisture with mass and motion fields can be accounted for. The result should be a more accurate representation of the initial moisture field.

Controversy has arisen over the importance of the initial specification of moisture in precipitation and moisture distribution forecast accuracy. In a study by Phillips (1978)[1], two fine mesh limited area models were run with two different moisture analyses, one of which fit the radiosonde values of moisture much better in an area adjacent to the Gulf of Mexico than the other. In both models much more realistic forecasts of vorticity and precipitation resulted in the Gulf area from using the analysis which was more representative of the observations. Apparently, the specification of too large values for humidity at mid-tropospheric levels resulted in the overdevelopment of cloudiness which in conjunction with the associated larger release of latent heat caused an overdevelopment of vorticity and excess

1. Phillips, N. A., 1978: A Test of Finer Resolution. Office Note 171, National Meteorological Center, National Weather Service, NOAA.

precipitation. van Maanen (1979)[2] describes an experiment conducted at the Europeon Centre for Medium Range Forecasts (ECMWF) in which three different sets of initial conditions are used in a five-day forecast using the ECMWF spectral model. The three sets of conditions were (a) mass, wind and humidity fields from the National Meteorological Center (NMC) analysis, (b) the ECMWF analysis for the same fields, and (c) the ECMWF in which the relative humidity was set at 60 percent for all model levels. Initial state (c) resulted in differences from (b) in five-day forecast fields of pressure and humidity that were of the same size as differences between forecasts using (a) and (b). The experiments were conducted for only one date, but assuming that the results hold for other dates, it was concluded that the specification of initial moisture is important out to at least five days of forecast time. By changing from an omni-directional successive correction humidity analysis to one which took into account the direction of humidity gradients, Atkins (1974)[3] demonstrated significant improvement in rainfall forecasts from a 10-level model for a specific weather event over western Europe. Her conclusion was that the quality of numerical short range forecasts of precipitation depends highly on the correctness of the initial specification of the humidity fields.

Somewhat different conclusions have been reached as a result of other studies. Smagorinsky et al. (1970)[4] attempted to determine which atmospheric variables had to be specified initially and which could be derived either diagnostically or were secondary in importance because of dynamic coupling in forecast models. Using the Geophysical Fluid Dynamics Laboratory (GFDL) nine-level hemispheric model for a particular set of initial conditions, a two-week integration was carried out. Then to test the importance of specification of initial humidity, another two-week integration was performed in which the only change in the initial conditions was to assign the relative

2. van Maanen, J., 1979: *Description of Some Properties of the Humidity Analysis Scheme in Use at the European Centre for Medium Range Weather Forecasts*. Verslagen, V-334, Koninkluk Nederlands Meteorologisch Instituut. (Available from NTIS)

3. Atkins, M. J., 1974: The objective analysis of relative humidity. Tellus, 26, 663-671.

4. Smagorinsky, J., K. Miyakoda, and R. F. Strickler, 1970: The relative importance of variables in initial conditions for dynamical weather prediction. Tellus, 22, 141-157.

humidity a value of 70 percent everywhere. Their results indicated that in extra-tropical latitudes there were no significant differences in the large scale variations of both relative humidity and accumulated precipitation after about 12 hours of forecast time. Their conclusion was that a proper specification of the horizontal wind field in the extra-tropical latitudes will set up those vertical velocity patterns that play the major role in the spatial distribution of moisture and precipitation in forecasts exceeding about 12 hours. Lejenas (1979)[5], in experiments with a primitive equation model covering the Northern Hemisphere down to 30°N, concluded that moisture initialization was only really important in assuring precipitation forecast quality in the first six hours of the forecast. His results suggested that vertical velocities implicit within the initial horizontal wind field are at least as important as fine detail in the moisture fields, especially for short term (<24 hour) forecasts, and that moisture specification is of little importance in longer term (>48 hour) forecasts for extra-tropical regions.

No attempt is made in this study to resolve the question of the importance of initial specification of moisture in numerical forecast models. Perhaps part of the apparent discrepancies in the studies mentioned above could be attributed to the individual cases studied, or more likely, to the differences in the forecast models used. An even more important problem, however, is the consistent deficiencies seen in precipitation forecasts from operational models which perform well in forecasting mass and motion fields over several days. Why dynamic coupling does not result in a consistently accurate forecast of precipitation in these models is a question that has not been satisfactorily answered. From the diversity of results from previous studies mentioned above, one may conclude that initial moisture specification is more important in some models than it is in others. Only tests performed in conjunction with a particular model over many cases can lead to concrete conclusions about the importance of initial moisture specification in that model.

If the initial specification of the moisture field is important for quality humidity and precipitation forecasts from at least some models, it seems that the most generally desirable objective would be to fashion the initial moisture field to most closely resemble the highest quality moisture observations. The mark of a good analysis scheme for a given model is the

5. Lejenas, H., 1979: Initialization of moisture in primitive equation models. Mon. Wea. Rev., 107, 1299-1305.

consistent production of the best forecast that can be achieved by that model. A good representation of the observations is an important requirement that an analysis scheme should meet in preparing data for the models that best simulate atmospheric processes. Model specific modifications may be necessary after this point, but the necessity of such modifications would be more a reflection on the reliability of the model than on that of the analysis. In fact, it may be more advantageous to modify or redesign a moisture analysis scheme once the properties of the spatial distribution of moisture are known, so that the scheme could consistently produce an analysis which reflects the unique variations within the moisture field that may prove important in preserving the accuracy of the predicted moisture and precipitation field.

For a global spectral forecast model, the proper specification of the wave structure of the moisture field is likely to be of greater importance than point-wise agreement with the observations. At the Air Force Geophysics Laboratory, a global spectral model of the moist atmosphere is being developed. In this model, particular importance will be placed on moisture physics and initialization, in an attempt to produce more skillful cloud forecasts in support of Air Force cloud-free line of sight requirements. Therefore, proper specification of initial moisture distribution will be an important prerequisite for spectral model integrations. To know how an objective analysis scheme must be designed to best represent the unique spectral characteristics of the spatial moisture variation, the spectral characteristics of the global moisture distribution must be known. This study examines the zonal and spherical harmonics of mass, motion, and moisture fields over periods of one week of summer data and one week of winter data. The results obtained from the study may then be applied in designing an analysis procedure that takes into account both the common and unique properties of global moisture distributions.

II. Description of Study

In a previous study (Gerlach, 1981[6]), two synoptic times were chosen for spectral analysis. The present study expands the data sample to two one-week periods: January 15 (00GMT) through January 21 (12GMT), 1978 (referred

6. Gerlach, A. M., Ed., 1981: Technique Development for Weather Forecasting. AFGL-TR-82-0020, Final Report, Contract F19628-81-C-0039, Systems and Applied Sciences Corporation (SASC), pp. 8-92.

to as JAN), and July 16 (00GMT) through July 22 (12GMT), 1978 (JUL). Global observations and analyses for 00GMT and 12GMT for each day in both periods were extracted from data tapes from the First GARP Global Experiment (FGGE)[7] of the Global Atmospheric Research Program (GARP). Level II-A and Level III-A data sets were used for the observations and the 2.5° latitude-longitude gridded analyses, respectively. These "A" sets contain only those observations that were received within a preset cutoff time and used for real-time FGGE purposes. In the present study, the Level II observations were used to "correct" the Level III analyzed fields in order to produce a grid point representation of the observations at each synoptic time. The method and motivation for the corrections will be described subsequently.

For each synoptic time, only radiosonde and pilot balloon observations from the Level II-A tapes were used. In addition, only those observations were used that satisfied the quality control checks performed on the FGGE data before they were put on tape. The resulting FGGE Level II-A observation values were plotted on mercator projection maps for 1/15/78 and 7/20/78, both at 00GMT. Examples of these maps including contours from hand-analysis are shown in Figs. 1a-1f. The maps are presented only to show the key synoptic features in the Northern Hemisphere for those times. The contours drawn over oceans and in the Southern Hemisphere are only estimates due to the sparsity of observations in these regions. The synoptic cases shown are typical of circulations observed in the two seasons, and as such are representative of normal seasonal conditions...

Before considering specific characteristics of these data sets, we first review several well known properties of global moisture fields. The zonally averaged structure of the specific humidity (q), for example, always reflects that of climatology; that is, zonally averaged q ($\bar{q}$) is a maximum at the equator and decreases monotonically toward both poles. Departures from the zonal mean for any given observation result primarily from either the longitudinal land mass distribution or disturbances in the zonal mean flow. The magnitude of the departures due to ocean-land distribution can be obtained from climatological studies.

Peixoto (1970)[8] conducted such a climatological study in which he plot-

7. Obtained from Department of the Air Force, OL-A, USAF Environmental Technical Applications Center (MAC), Federal Building, Asheville, NC 28801.

8. Peixoto, J. P., 1970: Water vapor balance of the atmosphere from five years of hemispheric data. Nordic Hydrol., 2, 120-136.

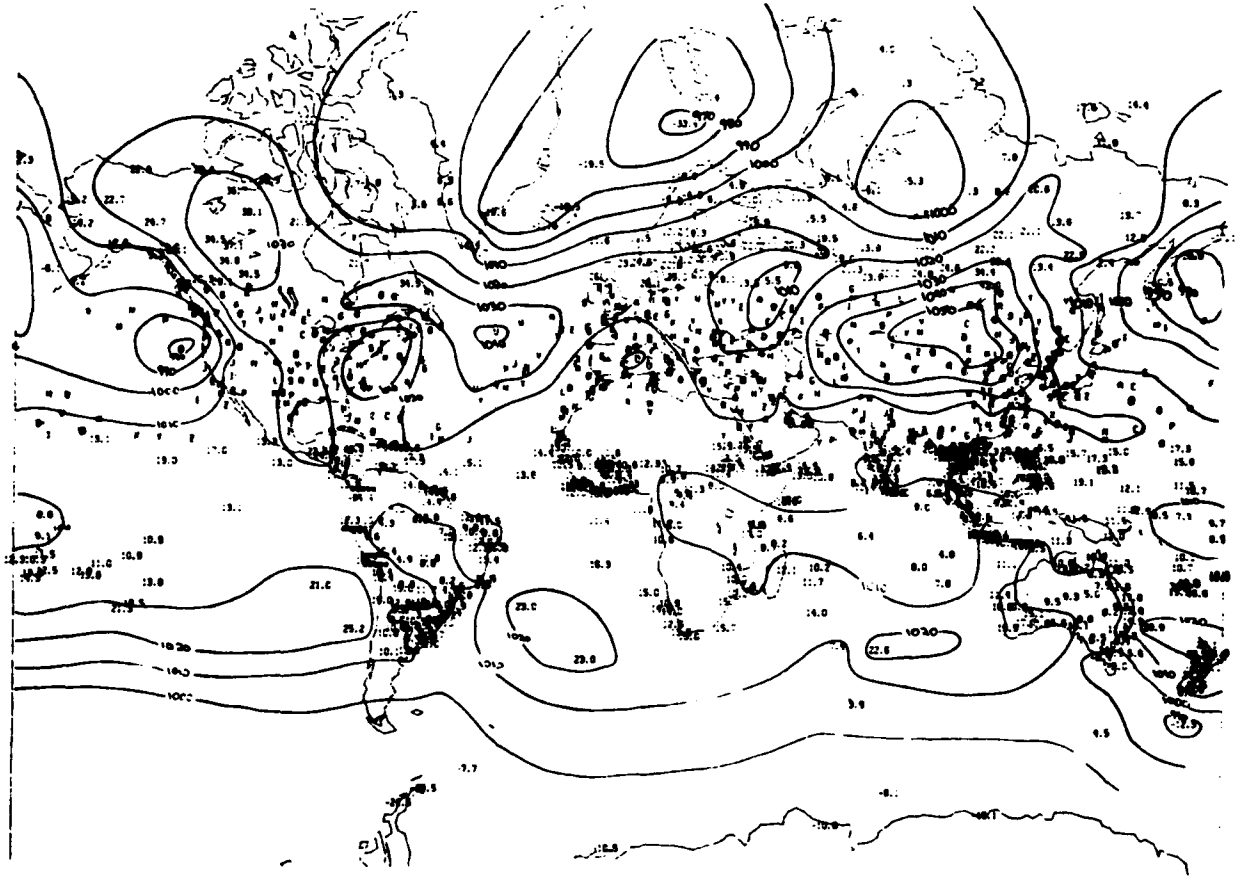

Fig. 1a. Subjective analysis of mean sea level pressure (mb) for 1/15/78 at 00GMT. Only rawinsonde and surface land/marine observations were used and only observations made within two hours of 00GMT (before and after) were included. Contours drawn over the oceans and Southern Hemisphere are not necessarily accurate.

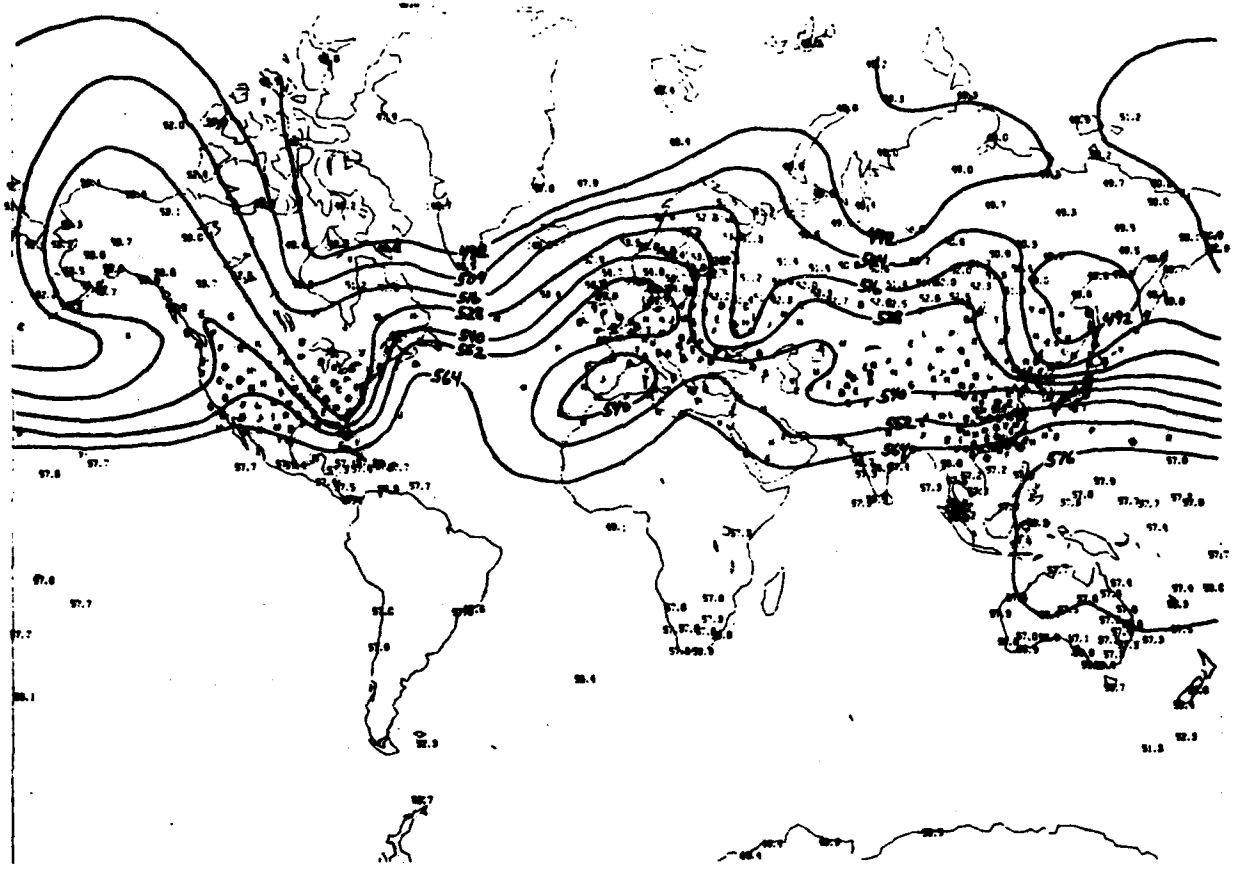

Fig. 1b. Subjective analysis of 500 mb geopotential height (dam) for 1/15/78 at 00GMT. Only rawinsonde and surface land/marine observations were used and only observations made within two hours of 00GMT (before and after) were included. Contours drawn over the oceans and Southern Hemi .. neces-sarily accurate.

Fig. 1c. Subjective analysis of 850 mb specific humidity (g kg^{-1}) for 1/15/78 at 00GMT. Only rawinsonde and surface land/marine observations were used and only observations made within two hours of 00GMT (before and after) were included. Contours drawn over the oceans and Southern Hemisphere are not necessarily accurate.

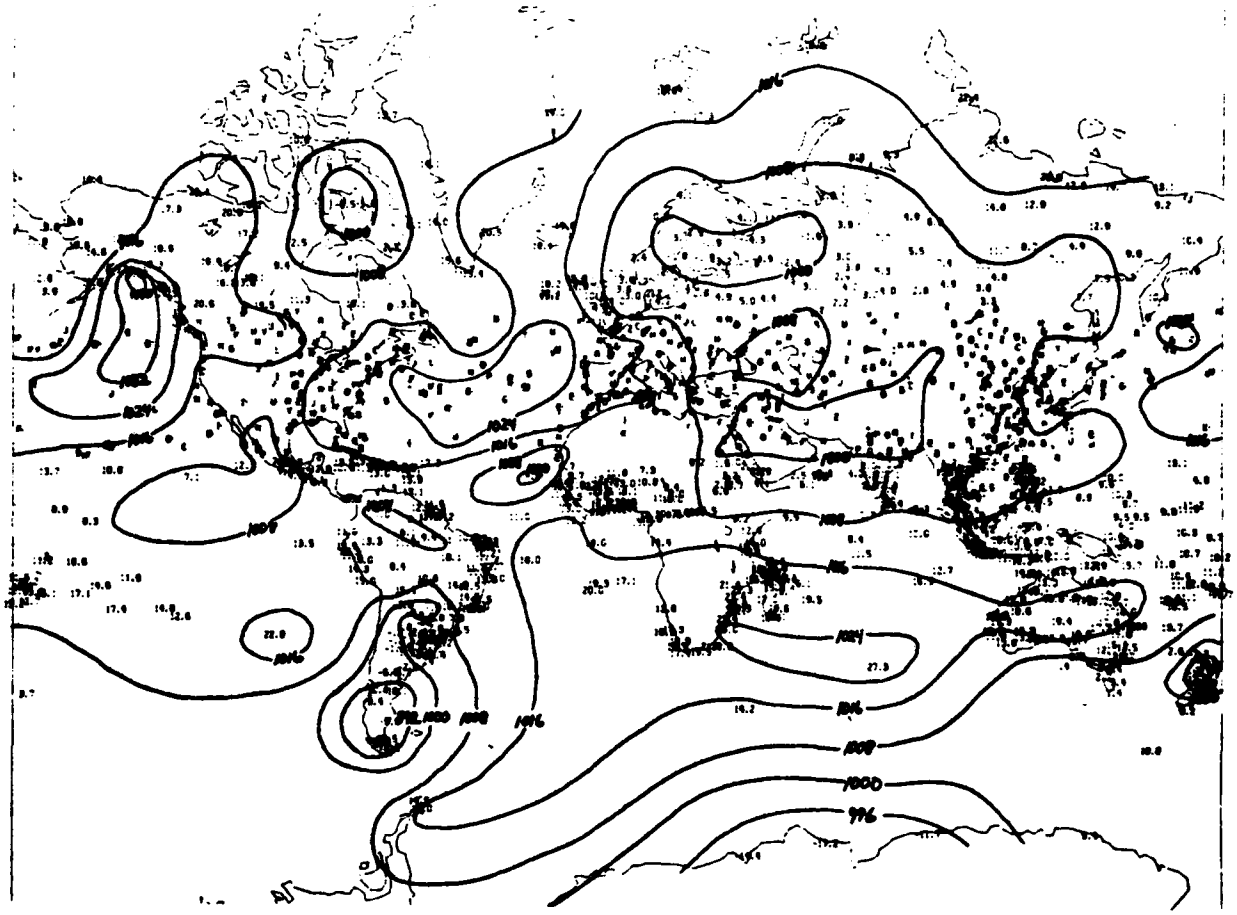

Fig. 1d. Subjective analysis of mean sea level pressure (mb) for 7/20/78 at 00GMT. Only rawinsonde and surface land/marine observations were used and only observations made within two hours of 00GMT (before and after) were included. Contours drawn over the oceans and Southern Hemisphere are not necessarily accurate.

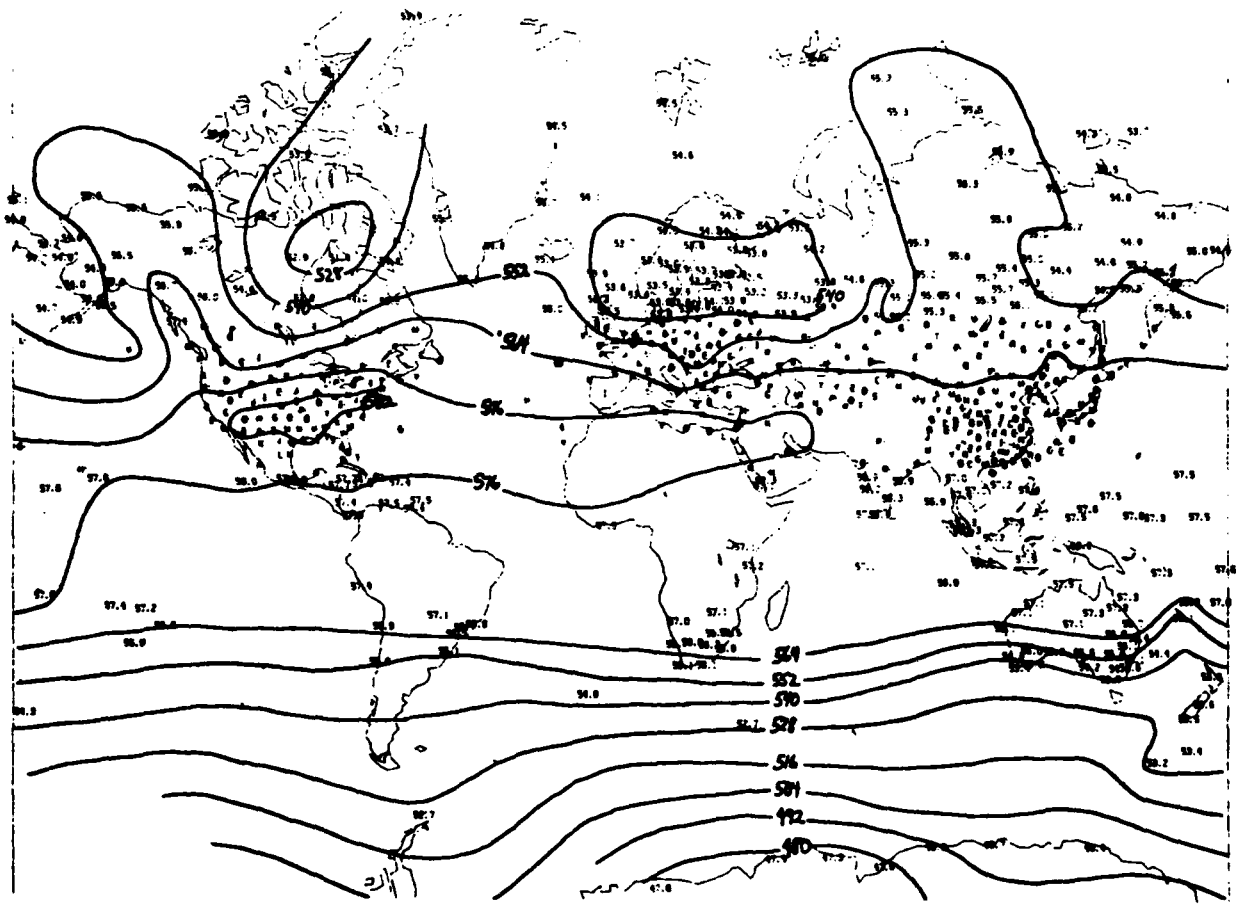

Fig. 1e. Subjective analysis of 500 mb geopotential height (dam) for 7/20/78 at 00GMT. Only rawinsonde and surface land/marine observations were used and only observations made within two hours of 00GMT (before and after) were included. Contours drawn over the oceans and Southern Hemisphere are not necessarily accurate.

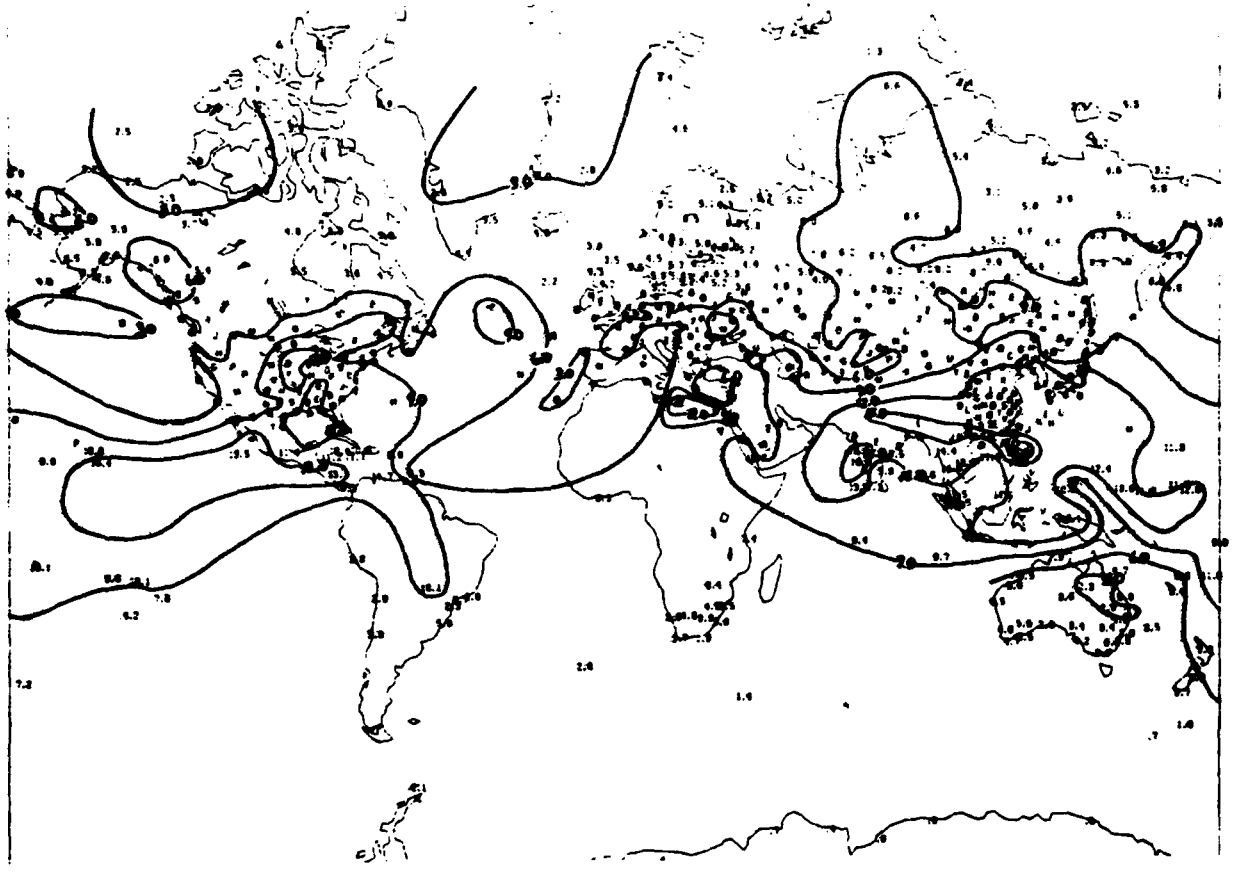

Fig. 1f. Subjective analysis of 850 mb specific humidity (g kg^{-1}) for 7/20/78 at 00GMT. Only rawinsonde and surface land/marine observations were used and only observations made within two hours of 00GMT (before and after) were included. Contours drawn over the oceans and Southern Hemisphere are not necessarily accurate.

ted the time-averaged vertically integrated precipitable water defined in terms of the time-averaged specific humidity $\hat{q}$ as

$$\hat{W} = g^{-1} \int_{sfc}^{300} \hat{q}\, dp \qquad (1)$$

where g is the acceleration due to gravity and p is pressure. His plot, taken from Rosen et al. (1979)[9], is reproduced in Fig. 2. By removing the zonal mean at each latitude from both the time-averaged field and the synoptic field, the departure due to orientation of ocean-land masses can be compared with that due to eddies. When this was done for the 1/15/78 00GMT case, calculations using q data for a station at 43.72°N and 65.25°W (near the moisture maximum associated with the northwest Atlantic storm) indicated a departure of precipitable water from the zonal mean for 45°N (computed from corrected q fields to be described later) of 2.3 x 10 kg m^{-2}. The largest departure from the zonal mean of the time-averaged values on Fig. 2 occurs at about 30°N (over the Sahara) and was calculated at -1.8 x 10 kg m^{-2} (using a time-averaged zonal mean computed from Oort and Rasmusson (1971)[10] for 30°N, yearly average). From this comparison it is clear that eddy departures can be as large as the largest time-averaged departures resulting from ocean-land distribution.

The moisture variables examined in this study were specific humidity and layer precipitable water. Relative humidity was not used because of its much higher degree of spatial irregularity. Initially, maps such as those in Fig. 1 were prepared for relative humidity, and it was obvious that the observations were characterized by many pockets of high humidity located adjacent to areas of low humidity. Such a discontinuous field is very difficult to analyze subjectively, and the ability of any objective analysis scheme to replicate such a highly irregular field is questionable.

Radiosonde observations of both temperature T and dewpoint depression D_p at mandatory and significant pressure levels were used in this study to calculate Level II values of q. To obtain corresponding values of W, the calculated values of q up to 250 mb were used in a numerical integration approximating the vertical integrals

9. Rosen, R. D., D. A. Salstein, and J. P. Peixoto, 1979: Variability in annual fields of large-scale atmospheric water vapor transport. Mon. Wea. Rev., 107, 26-37.

10. Oort, A. H., and E. M. Rasmusson, 1971: Atmospheric Circulation Statistics. NOAA Prof. Pap. No. 5 (NTIS Com-72-50295), 323 pp.

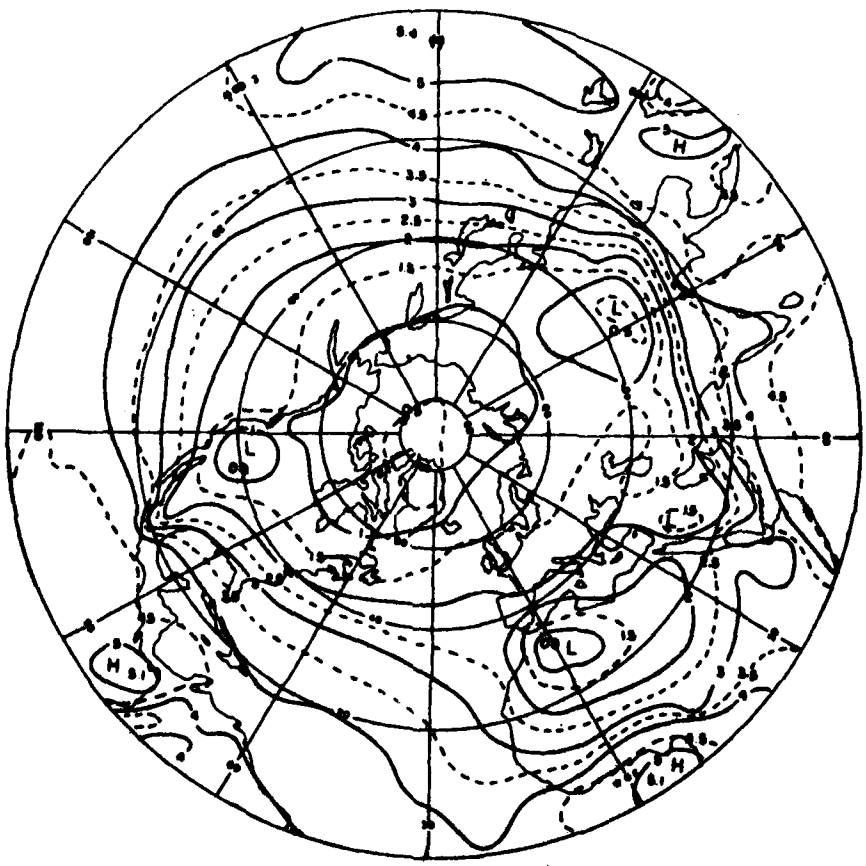

Fig. 2. Polar stereographic map of vertically integrated time mean precipitable water $\hat{W}$ for the period May 1, 1958 - April 30, 1963. Units for $\hat{W}$ are x 10 kg m^{-2} (from Rosen et al., 1979[9]; taken originally from Peixoto, 1970[8]).

$$W_{850} = \frac{1}{g\rho_0} \int_{sfc - 300}^{sfc} q \, dp \qquad W_{500} = \frac{1}{g\rho_0} \int_{300}^{sfc - 300} q \, dp \tag{2}$$

for each sounding (ρ_0 is the density of water, and W_{850} and W_{500} are computed in cm). The subscripts 850 and 500 are used only to indicate "lower" and "upper" layers; in most soundings they represent approximately the mid-levels of the two layers. The layers were chosen so that the mid-levels would coincide with the pressure levels at which the harmonic analysis was performed on the other quantities considered in this study.

To insure a sufficiently complete set of q values for the above integration at each sounding location, the following procedure was used. First, a check was made to determine if a q value existed at a pressure less than or equal to 300 mb. If not, a check was made to see if the highest level with a q value in that sounding was between 300 and 400 mb. If so, a value was extrapolated to 300 mb according to the formula

$$q_{300} = q_0 \, [1 - .695 \, (p_0 - 300)/100] \tag{3}$$

where q_0 is the specific humidity value at the highest pressure level p_0. Using specific humidity values at 300 and 400 mb from Oort and Rasmusson (1971)[10] representing zonal, yearly averages, the quotients $\hat{\bar{q}}_{300} / \hat{\bar{q}}_{400}$ were averaged over 5° latitude intervals from 0° to 75°N. An average value of .305 was obtained, from which the complement value of .695 was obtained. A linear variation was assumed between the two levels. At this point a test was performed to check if (a) the lowest pressure was $\leq p_{sfc} - 300$ mb, or (b) at least one value had a pressure ≤ 300 mb (including the extrapolated value if one had been added), or (c) both. The sounding was discarded if none of the above was true. For type (a), there had to be at least three values $\geq p_{sfc} - 300$ mb, and the lowest p value had to be ≤ 700 mb in order for the sounding to be used. Case (b) required at least three values with pressures such that $300 \leq p \leq p_{sfc} - 300$ for the sounding to be used. A minimum of three levels was also required for case (c). A cubic spline was then used to interpolate values of q at even multiples of 50 mb between the highest and lowest pressure value in the sounding. Using the given and interpolated values (and extrapolated 300 mb values where they exist), the integrals (Eq. (2)) were evaluated using the trapezoidal rule. When negative values of q were generated from the cubic spline (which generally occurred in less than 10 percent

of the accepted soundings for an observation period in this study), the negative values were replaced by assuming a linear variation of q with pressure between the non-negative values immediately above and below the negative value or values.

The same basic scheme was used to calculate W_{850} and W_{500} for Level III values, except in this case a) analyzed values of T and RH were available to calculate q at mandatory pressure levels only, and b) the surface pressure values needed in Eq. (2) had to be derived. To derive surface pressure, analyzed mean sea level pressure and terrain height values were used with analyzed geopotential heights to interpolate values of surface pressure for each grid point. The interpolation was based on the assumption that geopotential height is a quadratic function of the natural logarithm of pressure, following the practice of the NMC. The cubic spline was then used to obtain values of q at even multiples of 50 mb between 1000 mb and 300 mb, at $p_{sfc} \leq 1000$ mb, and at $p_{sfc} - 300$. In cases where $p_{sfc} > 1000$, q_{sfc} was set equal to q_{1000}. The interpolation and integration was performed in the same way as for the Level II data.

To perform zonal and spherical harmonic analyses, global grid point representations of the observations had to be prepared. In choosing a method to combine analyses and observations into a gridded field, it was important to minimize the modification of the true spectral character of the atmospheric field. This was why a direct interpolation of observations onto grid points was not used, since most polynomial-type direct interpolations have a bias toward certain wave numbers (Yang and Shapiro, 1973[11]). On the other hand, the Flattery analysis itself, used to prepare the Level III analyses, also includes certain biases that, without attempted correction, would influence the harmonics to be observed here in the results. For example, the Flattery analysis includes a truncation at zonal wave number 24, even though the Level III analysis values are available at 2.5^{o} latitude-longitude intervals, which would allow resolving waves as small as zonal wave number 72. Furthermore, the Flattery analysis uses 12-hour forecasts from the National Meteorological Center's coarse-grid hemispheric model as the basis for the first-guess field. The Flattery scheme is iterated several

11. Yang, C. H., and R. Shapiro, 1973: The effects of the observational system and the method of interpolation on the computation of spectra. J. Atmos. Sci., 4, 530-536.

times, beginning with the expansion in terms of just the lowest wave numbers, and including higher wave numbers with successive iterations. (This is analogous to the successive approximation techniques that use successively larger scan radii in the selection of observations to influence the value at a grid point.) In addition, Chu and Parrish (1977)[12] showed that a simple scheme that transfers data to grid points resulted in a humidity field that better represented observations than the Flattery analysis (described by Cooley, 1974[13]) for a case over the eastern U. S. While admittedly the emphasis in the present study is on spectral representation of the observations rather than point-wise accuracy, the nature of the larger point-wise error shown in their study clearly would have a negative impact on the spectral representation. Despite these shortcomings of the Flattery analysis, it has the favorable property that it lacks any distinct bias toward individual groups of waves, since it is based on an expansion of the data in unweighted Hough basis functions. For this reason, the Flattery analyses were used as the first guess field, and each corresponding set of observations was used to correct the field in successive scans univariately using the well known method of Cressman (1959)[14]. In this way, corrected fields of zonal wind (u), meridional wind (v), temperature, geopotential height (Z), specific humidity, and layer precipitable water (W) at both 850 mb and 500 mb levels were prepared for each of the 14 observation times in the two periods.

To measure the impact of the corrections, two quantities were then calculated for each of the two fields. The original Flattery analyzed field (FG) and the final corrected field (CFG) were interpolated bilinearly to the observation locations for comparison with the observed values (OB). Then the following two root mean square error quantities were calculated for each field:

$$R_{CFG} = \left[\frac{1}{N}\sum_{i=1}^{N}(CFG_i - OB_i)^2\right]^{\frac{1}{2}} \qquad R_{FG} = \left[\frac{1}{N}\sum_{i=1}^{N}(FG_i - OB_i)^2\right]^{\frac{1}{2}} \quad (4)$$

12. Chu, R., and D. Parrish, 1977: Humidity Analyses for Operational Prediction Models at the National Meteorological Center. Office Note 140, National Meteorological Center, NWS, NOAA.

13. Cooley, D. S., 1974: A Description of the Flattery Global Analysis Method - No. 1. Tech. Proc. Bul. No. 105, NWS, NOAA.

14. Cressman, G., 1959: An operational objective analysis system. Mon. Wea. Rev., 87, 367-374.

where N is the number of observations used in each field for correction of the first guess. The quantity $r = 1 - (R_{CFG}/R_{FG})$ is a measure of the impact the observations had in modifying the analyzed field to be more representative of the observations; the closer r is to unity, the more the corrected field is like the observed field with respect to the first guess. Values for N and r averaged over the 14 observation periods for each quantity, level, and month are presented in Table 1.

TABLE 1. AVERAGE NUMBER OF OBSERVATIONS (N) AND ROOT MEAN SQUARE ERROR RATIO (r)

DATE	LEVEL		u	v	T	Z	q	W
JAN	850	N	810	810	608	613	587	596
		r	.36	.36	.45	.46	.61	.62
	500	N	718	718	624	620	545	465
		r	.32	.33	.38	.45	.60	.62
JUL	850	N	848	848	618	616	601	629
		r	.37	.34	.42	.45	.51	.44
	500	N	762	762	640	634	564	554
		r	.33	.35	.34	.44	.43	.46

In most cases, the table shows that the correction had a somewhat greater impact on T and Z than on u and v, with a still greater change for q and W. The use of fewer vertical empirical orthogonal functions in the Flattery humidity analysis might be suspected of creating a first guess humidity that was more unlike the observations than the first guess fields for the other quantities. However, in the previous study (Gerlach, 1981[6]) it was shown that the first three vertical modes, the ones used in the humidity analysis, contain 80-90 percent of the total horizontal variance when complete radiosonde observations were analyzed following the vertical expansion method used in the Flattery analysis. Therefore, it is unlikely that the greater change in the humidity fields can be explained by the use of fewer vertical modes to create the first guess field. Actually, no clear explanation can be given for the trends in the r values in Table 1. However, although as a group they show that substantial point-wise changes result from the observational corrections, the corrected fields still are for the most part more a product of the first guess than they are of the observations. Apparently, the number of observations used is not the strongest factor in determining the amount of change brought about by the corrections. In fact, just the opposite seems to be the case, and this may be explained by the fact that more

observations available in the Flattery analysis would result in a better representation of the observations by the first guess. Then the change brought about by the observations would be expected to be smaller. The effect on these results from the interpolation to observation sites is not considered. A better method would have been to use the coefficients of the Flattery expansion to reproduce Flattery values at the observation sites, but these coefficients were not available.

III. Harmonic Analysis of Corrected Fields

Each of the corrected fields was analyzed spectrally using both zonal and spherical harmonic expansions. To prepare each field for these expansions, the departure from the global average was calculated for each of the grid points of the 2.5° latitude-longitude global grid. The global average of each quantity was calculated by evaluating the integral

$$[A] = \tfrac{1}{2} \int_{-\pi/2}^{\pi/2} \bar{A}\ (\phi)\ \cos\ \phi\ d\phi \tag{5}$$

using a Gaussian quadrature integration in the form

$$[A] \simeq \tfrac{1}{2} \sum_{k=1}^{64} \bar{A}_k W_k \tag{6}$$

where ϕ represents latitude, $\bar{A}$ represents the zonal mean of the quantity, (computed as the arithmetic average of the 144 points around each latitude circle), and W_k are the Gaussian weights corresponding to each of the 64 Gaussian latitudes used in the study. The $\bar{A}\ (\phi)$ values at every 2.5° latitude were interpolated linearly to the Gaussian latitudes, the quadrature was performed, and the departure value $A^*\ (\phi,\lambda) = A\ (\phi,\lambda) - [A]$ was calculated for each grid point.

Each departure field was expanded along each 2.5° latitude using the harmonic expansion of the form

$$A^*\ (\phi,\lambda) = \sum_{m=0}^{M} [a_m(\phi)\ \cos\ m\lambda + b_m(\phi)\ \sin\ m\lambda] \tag{7}$$

where λ is longitude and m is the zonal wave number out to M = 72. The coefficients were obtained using a fast Fourier transform algorithm.

The zonal mean power a_0^2 and the zonal eddy power $a_m^2 + b_m^2$, m = 1, 72 were calculated for each latitude for each quantity, level, and time, and were then averaged over time. The weekly averaged values of total eddy power were normalized in the form

$$\Gamma_m(\phi) = \frac{\{a_m^2 + b_m^2\}}{\sum_{m=1}^{M} \{a_m^2 + b_m^2\}} \qquad (8)$$

where the brackets {} represent the weekly averaged quantity. Thus the fractional contribution Γ_m over all wave numbers for a particular latitude should add up to unity.

Before discussing the results, a comment should be made about the sensitivity of the spectra of the corrected field to the density of observations. With the addition of more observations, the largest changes in the spectra would be seen in the high wave numbers, since a greater density of observations would allow the resolving of smaller waves in the fields if they exist. The long waves are probably already well represented by the existing less dense data coverage, so large relative changes in the low wave numbers would not be expected by the addition of other types of observations, such as those from satellites. The question is whether the present data may produce spectra that are more representative of the actual wave structure for one quantity than they are for another. In this regard, for example, the rawinsonde network might be adequate for depiction of the true spectral characteristics of the height field but may not be sufficiently dense to resolve important contributions from high wave numbers in the q field. A sensitivity study of the effect of additional observatons on the various spectra was not included in this study, but it would be useful in verifying the general conclusions reached in the present project.

Values of weekly averaged zonal mean power $\{a_0^2\}$ and zonal eddy power $\sum_{m=1}^{M} \{a_m^2 + b_m^2\}$ are shown graphically in Figs. 3a-d. The zonal mean power curves for T, Z, q, W are similar in that they all show the maximum positive departure from the global average at the equator and maximum negative departure at the poles. The two minima in the curves are at or near the latitudes where the zonal mean of the quantity is equal to the global mean. Zonal mean power curves for u and v do not show this characteristic variation. The u variation reflects the latitudinal variation of the westerlies at temperate latitudes and easterlies in tropical latitudes. The zonally-averaged departure from the global mean for v is an indicator of the poleward-equatorward mass flux at each level, a small quantity.

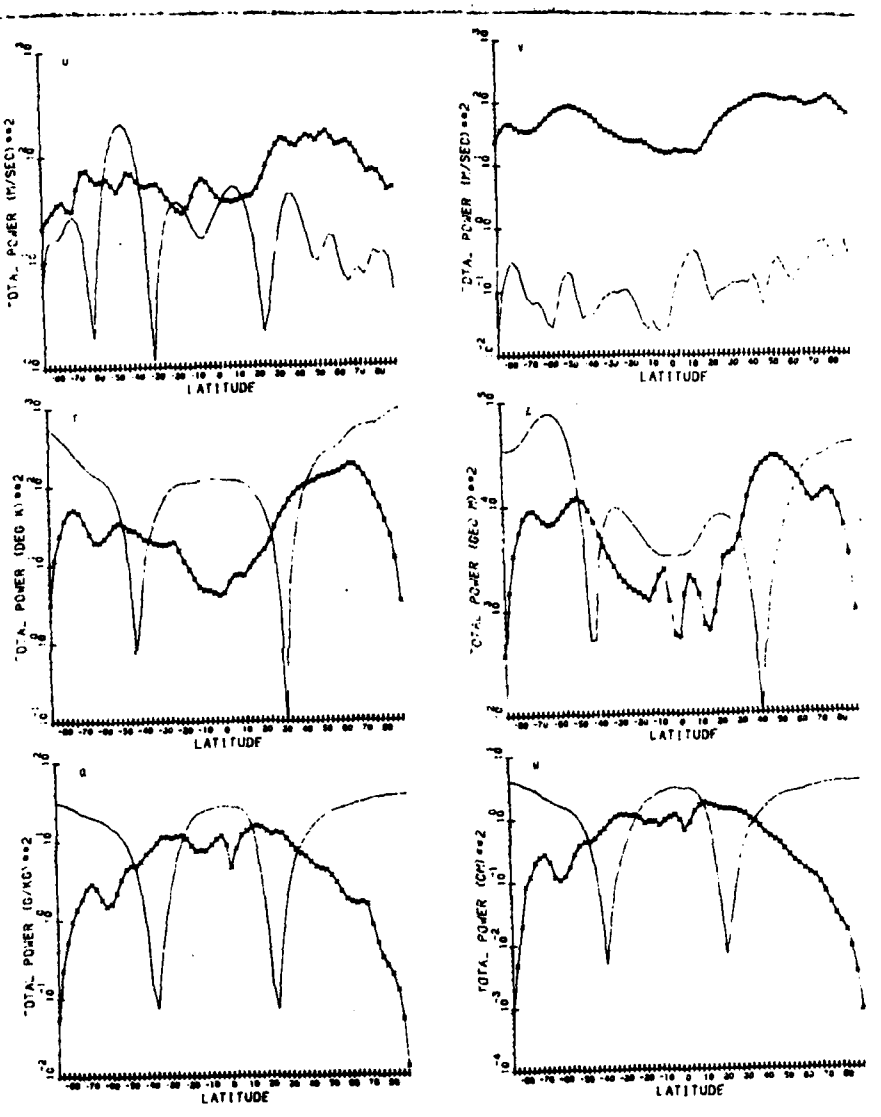

Fig. 3a. Weekly averaged zonal mean power ——— and zonal eddy power x—x—x for JAN at 850 mb.

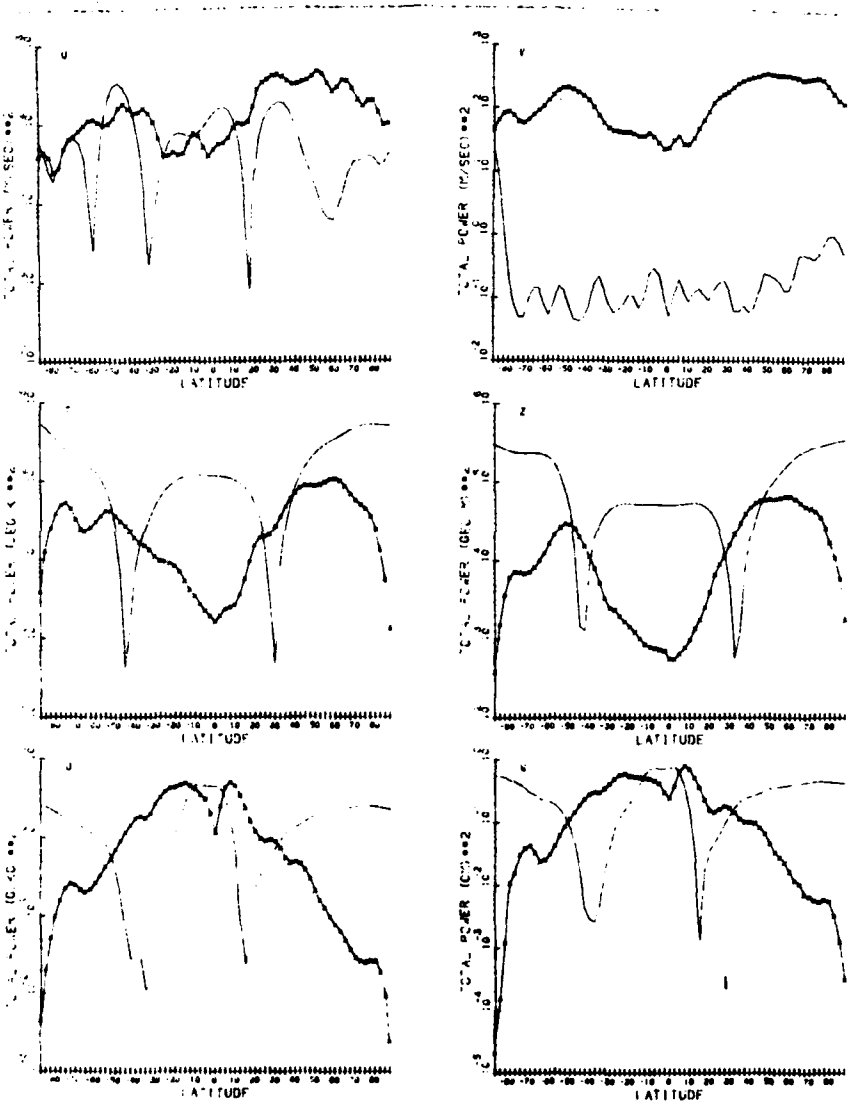

Fig. 3b. Weekly averaged zonal mean power ——— and zonal eddy power x—x—x for JAN at 500 mb.

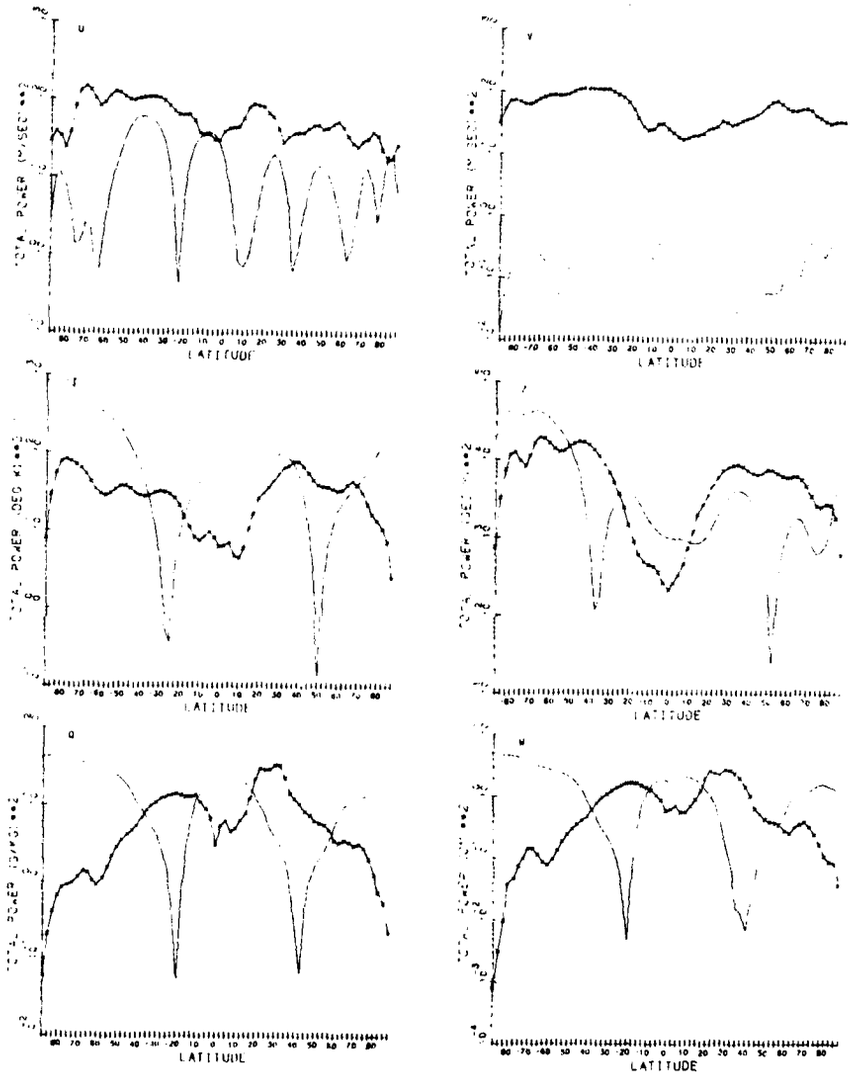

Fig. 3c. Weekly averaged zonal mean power ——— and zonal eddy power x—x—x for JUL at 850 mb.

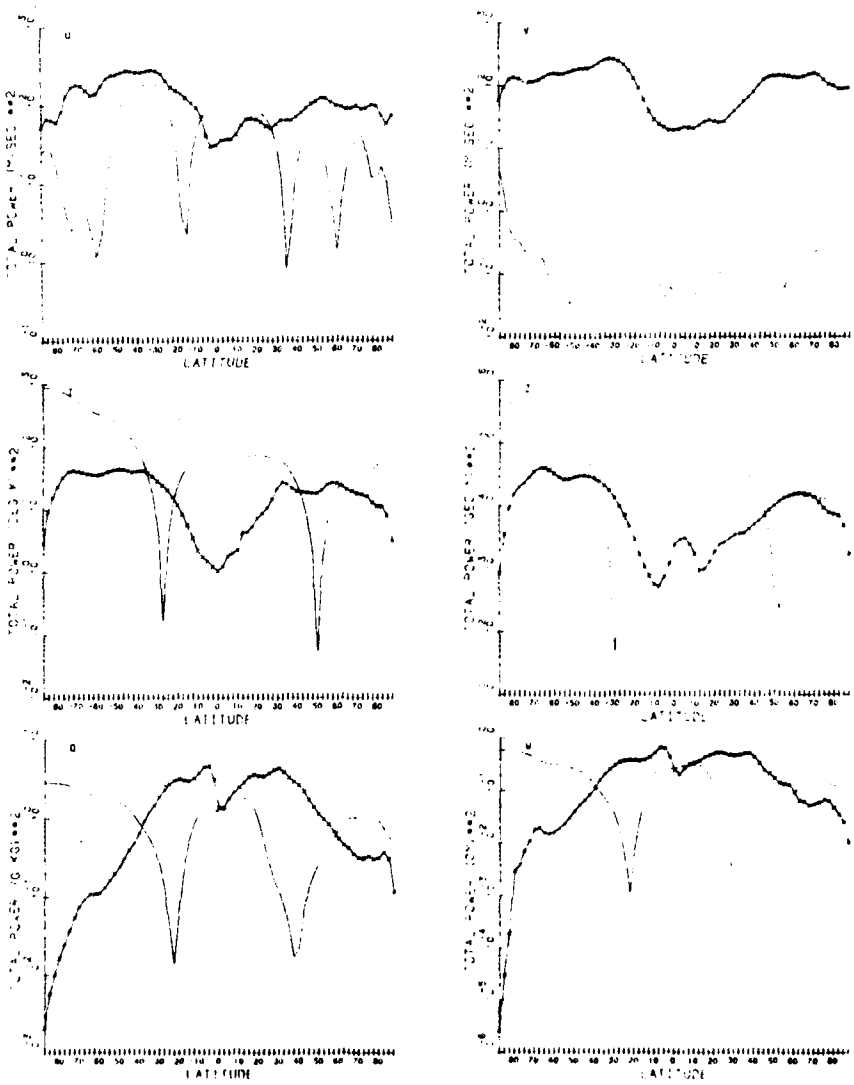

Fig. 3d. Weekly averaged zonal mean power ——— and zonal eddy power x—x—x for JUL at 500 mb.

For all plots of $\{a_0^2\}$ for T, Z, q, and W, the winter hemisphere minimum is closer to the equator than the summer hemisphere minimum. This means that the zonal average of each quantity decreases to the global average faster with latitude in the winter hemisphere than it does in the summer hemisphere. This makes sense since the average winter hemisphere value of T, Z, q, and W is less than the summer hemisphere value. When the locations of the minima are compared for a given month at a given level, however, it is clear that both the summer and winter hemisphere minima are closer to the equator for q and W than they are for T and Z. When the zonal averages were plotted as a function of latitude for T, Z, and q for 1/15/78 at 00Z, q showed a much more rapid decrease with latitude in both hemispheres than did the other two quantities. This steeper meridional gradient accounts for the closer position of the zonally averaged global mean departures to the equator for q and W. The latitudinal difference between the summer and winter hemisphere minima decreases significantly with height for q and W, mostly due to the movement of the winter hemisphere minimum to lower latitudes. This shift is not nearly as pronounced in T and Z. This indicates that the magnitude of the winter hemisphere meridional gradient of the moisture variables must increase with height, unlike that of the temperature and height fields.

The total zonal eddy power curves for T and Z show a bimodal character, with maxima at mid-latitudes and minima at the equator and both poles. This is also true to a lesser extent of the u and v distributions. This is not surprising due to the large amplitude eddies which form in and propagate in the westerlies at mid-latitudes. In contrast to this is the latitudinal distribution of zonal eddy power for q and W, which shows a maximum at the equator and minima at the poles. Apparently, the amplitudes of the departures from the zonal mean over all length scales are greater in the tropics than those in mid-latitudes. Two possible explanations for this are (a) the restriction of the amplitude of q (and thus W) about the zonal mean resulting from the saturation specific humidity q_s which is lower in the mid-latitudes than it is in the tropics, and (b) the larger magnitude of stationary departures from the zonal mean of q and W (due to land-ocean distribution) in the tropics. Dealing with the latter possibility first, one could measure the contribution of this effect by removing the time-averaged component from each of the fields and performing the same zonal harmonic analysis of the time departure fields, then comparing the resulting total

eddy power curves with those of Fig. 3. However, the one-week time period used in each case would probably not be a sufficient length of time to assure that the time-average is representative of climatological conditions. Using the climatological values of $\hat{W}$ in Fig. 2 along with vertically integrated values of $\bar{q}$ from Oort and Rasmusson (1971)[10] for a yearly average, the largest apparent departure from the zonal mean south of 20°N was about 2.0 x 10 kg m^{-2}, compared to a departure of 1.2 x 10 kg m^{-2} at 40°N. In fact, the largest departure of the time-averaged field from the zonal mean occurs at 30°N, most likely resulting from the Sahara. This large departure shows up at 30°N on the zonal eddy power plots in Figs. 3a and 3c for q and W, expecially in the JUL case. The fact that at least qualitatively the time averaged departures below 20°N are not significantly larger than mid-latitude zonal departures and that the 30°N maximum shows up as just a prominence on already large low latitude values of eddy power for q and W suggests that factor (b) is not primarily responsible for the general shape of the q and W curves.

To consider the case for the first explanation, consider another effect of a lower q_s value resulting from lower temperatures. By comparing the right hand sides of the zonal power curves for JAN with the corresponding section of curve for JUL (the Northern Hemisphere sections are compared due to their higher observation density), it is clear that for u, v and especially T, Z, the total zonal eddy power (area under the curve for NH) is greater for the winter hemisphere than it is for the summer hemisphere. Again, this is not surprising because the amplitudes of large-scale wave disturbances are clearly larger in the winter hemisphere due to greater baroclinicity. However, the q and W power curves show greater zonal eddy power in the summer hemisphere. It appears that higher values for the q and W curves are favored in warm regions and lower values in the cooler regions. Thus, it could be that the lower temperatures tend to reduce the total variance about the zonal mean because of the limiting value of q_s which decreases with decreasing temperature. Clear support for this argument can be gained from Table 2. The corrected fields of T for 00GMT on 1/15/78 for both levels were used to generate fields of saturation specific humidity q_s. Then the q fields for the same time and date, whose zonal power curves look very much like the weekly average curves in Fig. 3, were used with the q_s fields to form RH = q/q_s at each grid point. The Northern Hemisphere average values show that while temperature increases by only 4 percent between

winter and summer, the saturation specific humidity q_s, acting as an upper limit for q, increases by 73 percent at 850 mb and 59 percent at 500 mb. For 850 mb, this translates to a maximum allowable departure from the average in q of 2.6 g/kg in the winter compared to 4.9 g/kg in the summer. The hemispheric average relative humidity is more like the temperature, in that there is very little change between the seasons. This suggests that the limiting magnitude of the departure about the mean for relative humidity is not nearly as sensitive to temperature as it is for specific humidity.

TABLE 2. NORTHERN HEMISPHERE AVERAGES

		$q(g\ kg^{-1})$	$T(^{o}K)$	$q_s(g\ kg^{-1})$	RH
850	1/15/78	5.35952	276.49600	8.00103	.66985
850	7/20/78	8.95516	288.18456	13.83457	.64730
500	1/15/78	1.23598	254.71750	2.67001	.46291
500	7/20/78	2.13636	267.28384	4.25537	.50204

Further evidence for the importance of the greater limiting influence of q_s can be gained from Figs. 4a-d, the zonal eddy power curves of RH for 1/15/78 and 7/20/78. Two facts can be noticed: (a) the total power in the winter hemisphere is as large as that for the summer hemisphere, and (b) the equatorial maximum seen in the q and W curves is not evident in the RH curves. In fact, there is indication of a bimodal character in the curves as in the T and Z curves, especially at 850 mb. The table values and curves would appear to explain that the variance of q in colder regions is held down by the lower value of q_s, and that relative humidity is not so strongly affected by this temperature limitation.

Values of Γ_m, the normalized (fractional) zonal eddy power, are contoured in $\log_{10}$ form (solid contours) in Figs. 5a-d. Only the values for the first 32 zonal wave numbers were included in the plots, since power contributions from higher wave numbers were negligibly small. The contours are labeled by the power of 10 corresponding to the fractional contribution to the total eddy power at a particular latitude by a particular wave number. For example, a point lying to the left of the -2 contour indicates that that wave number contributes at least one percent of the total power at the corresponding latitude. The dashed curves represent equatorial wave number — any point lying along a given curve represents a constant wavelength equal to the wavelength corresponding to that number of waves around the equator. The dashed curves were included because it was evident that the normalized power contours generally followed wavelength rather than local wave number.

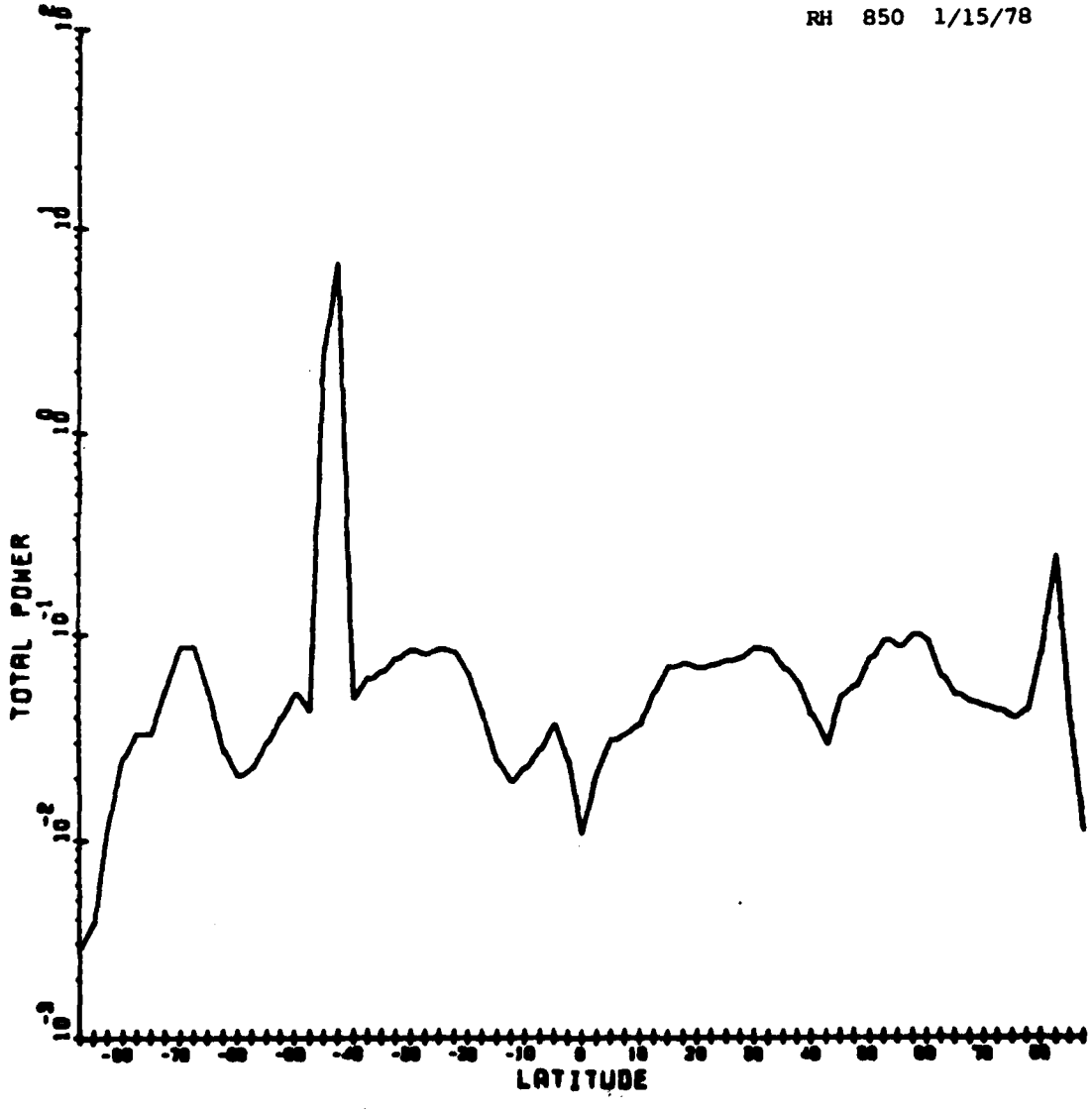

Fig. 4a. Total zonal power for the departures from the zonal average for the ratio q/q_s. Both q and T used in the calculations are the corrected field values.

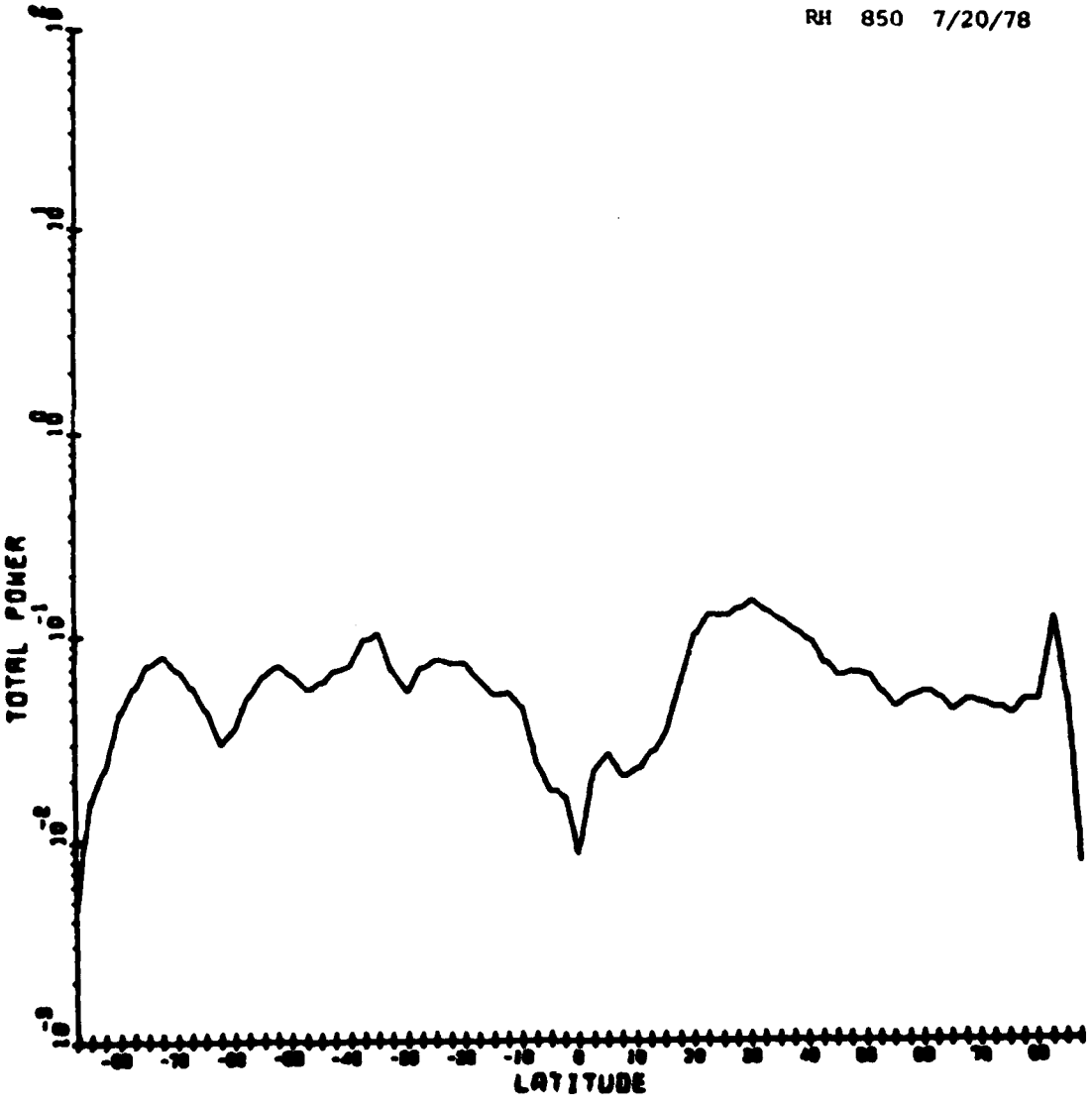

Fig. 4b. Total zonal power for the departures from the zonal average for the ratio q/q_s. Both q and T used in the calculations are the corrected field values.

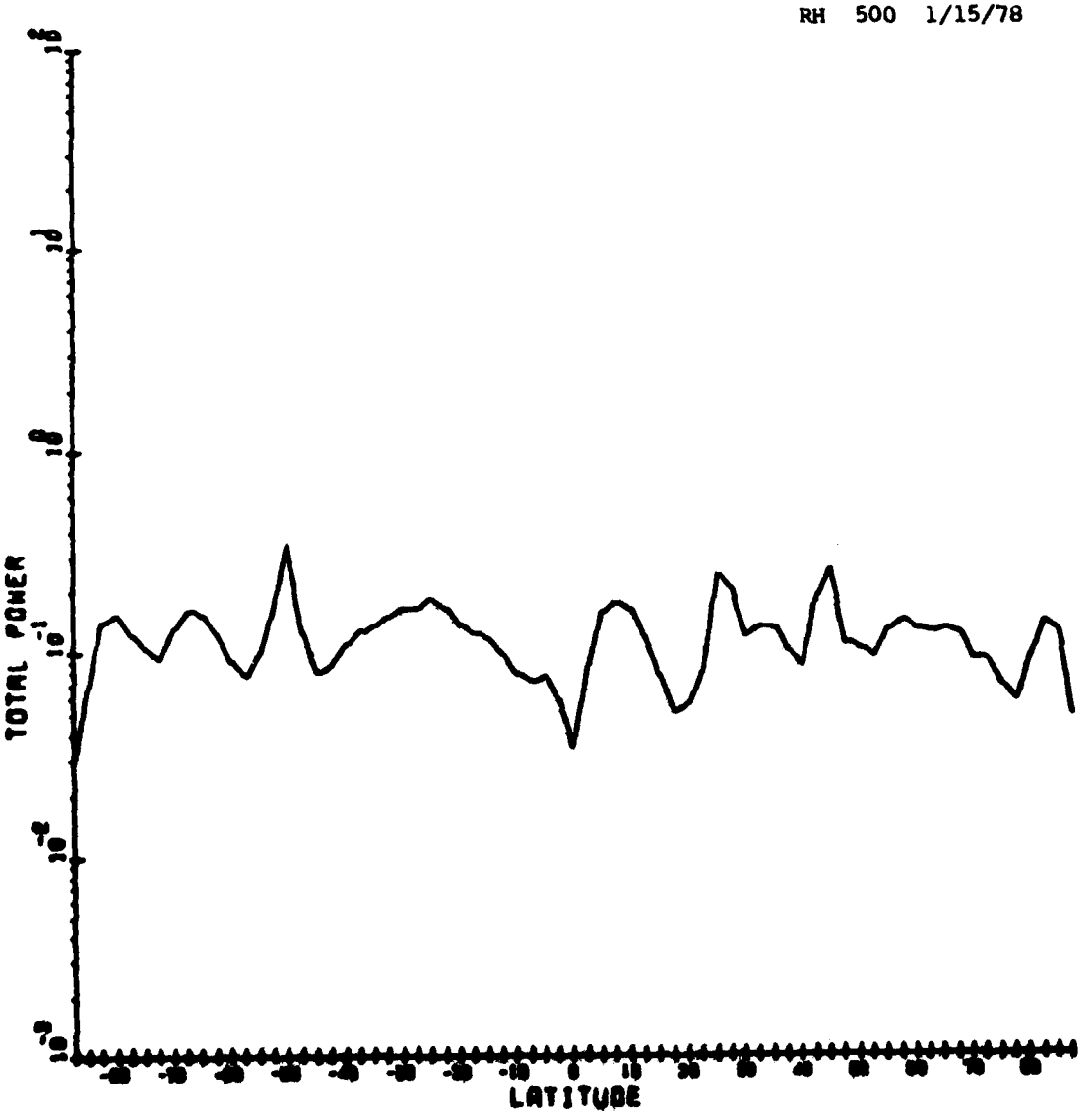

Fig. 4c. Total zonal power for the departures from the zonal average for the ratio q/q_s. Both q and T used in the calculations are the corrected field values.

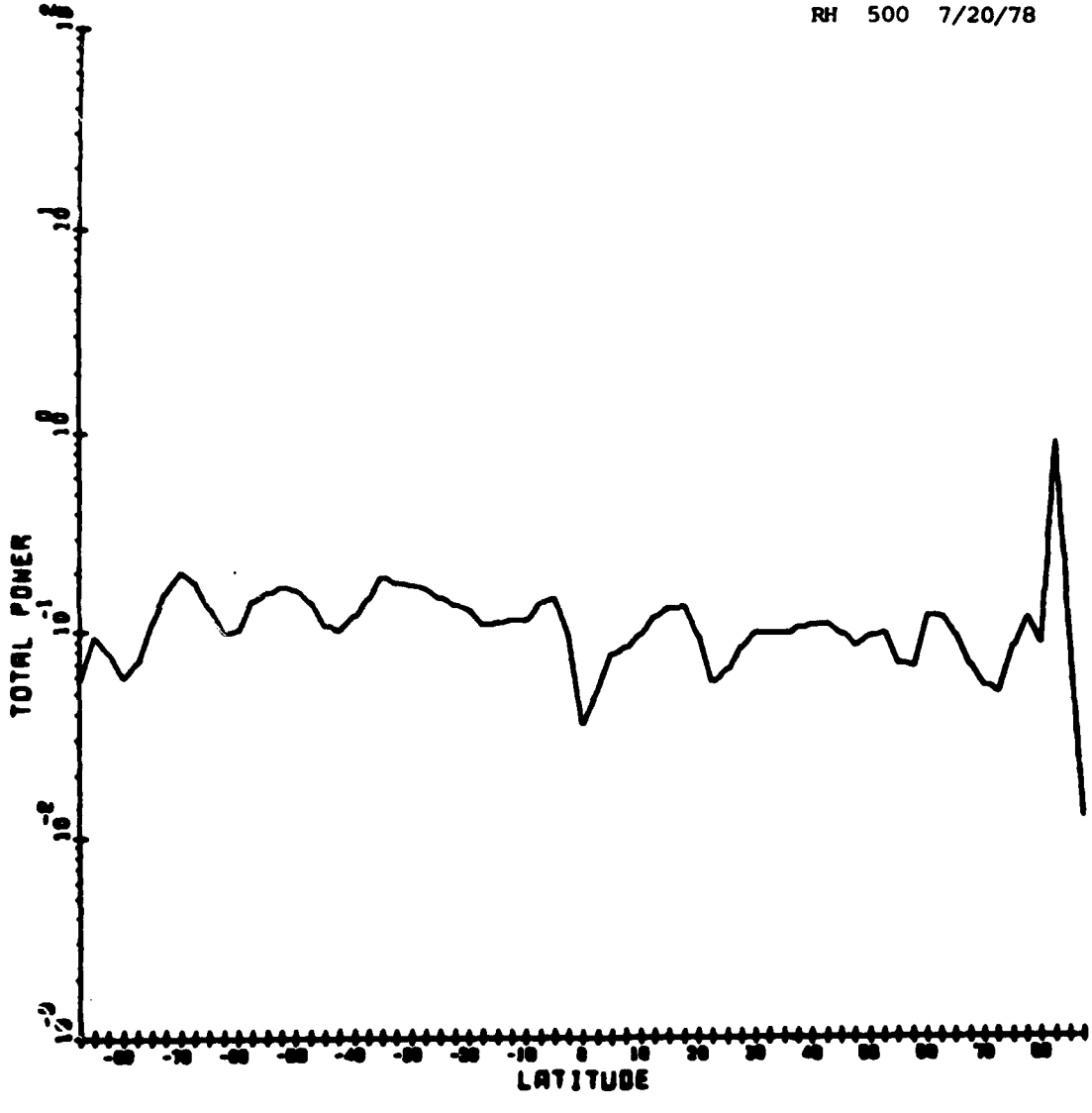

Fig. 4d. Total zonal power for the departures from the zonal average for the ratio q/q_s. Both q and T used in the calculations are the corrected field values.

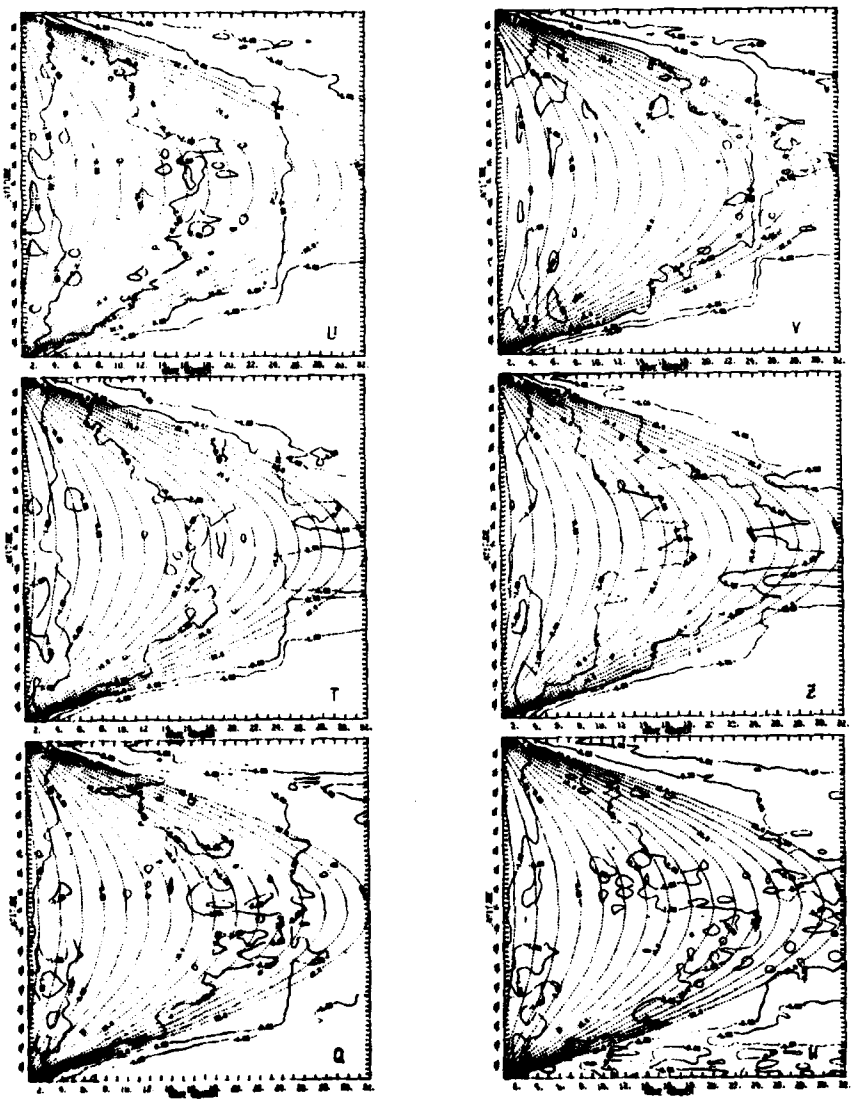

Fig. 5a. Weekly averaged normalized zonal eddy power for JAN at 850 mb. Contour labels are powers of 10 corresponding to the fractional contribution of each wave number. Dashed curves represent lines of constant equatorial wave number, given by the contour labels.

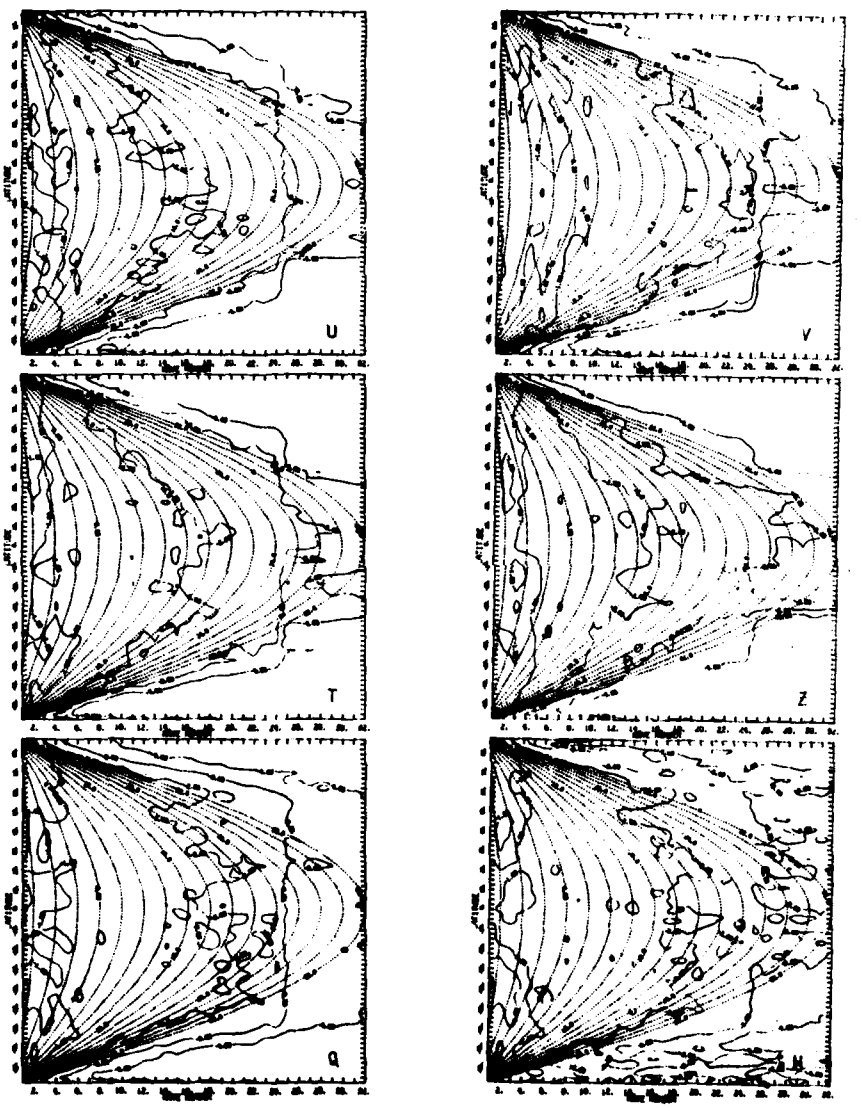

Fig. 5b. Weekly averaqed normalized zonal eddy power for JAN at 500 mb.

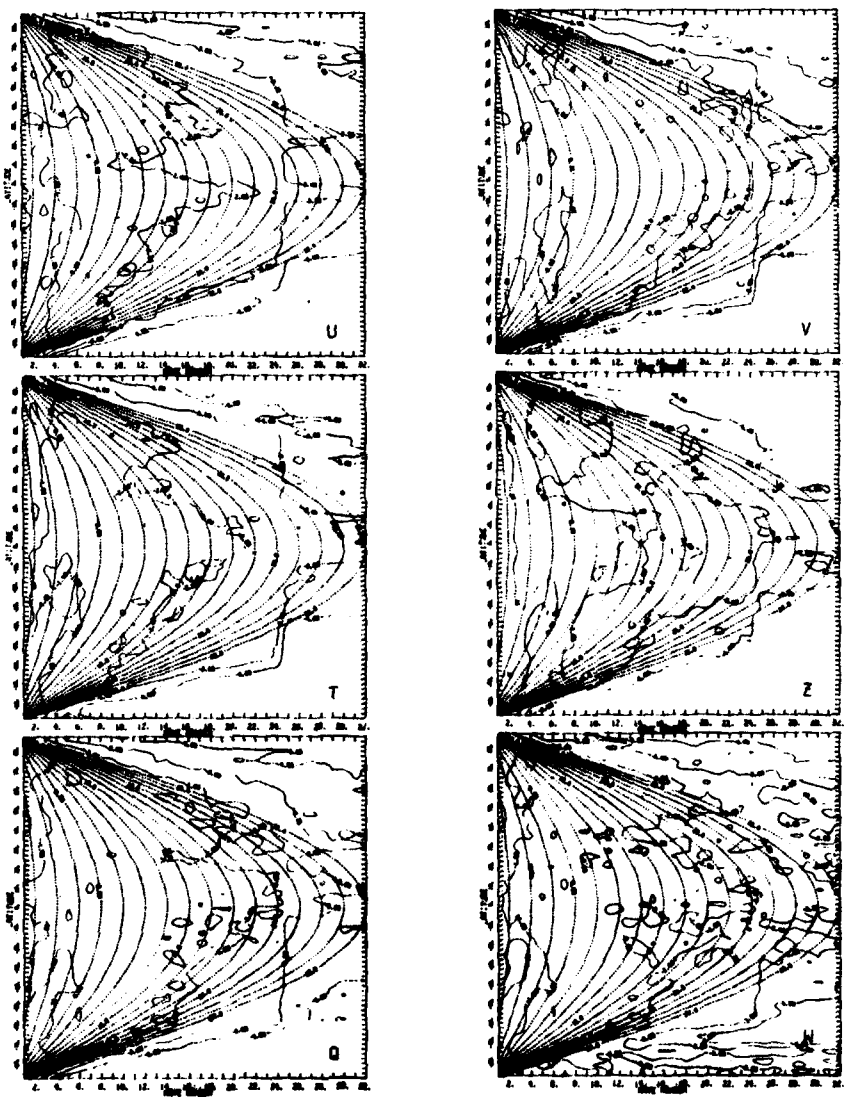

Fig. 5c. Weekly averaged normalized zonal eddy power for JUL at 850 mb.

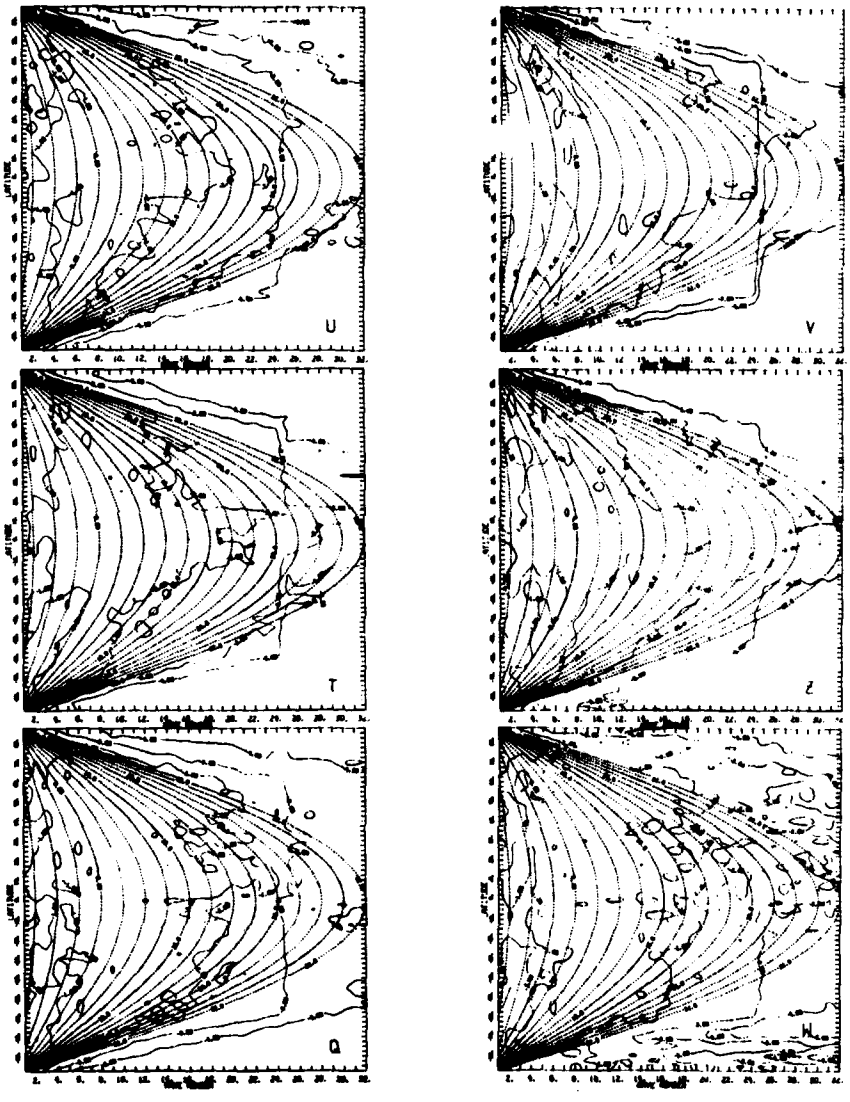

Fig. 5d. Weekly averaged normalized zonal eddy power for JUL at 500 mb.

This is especially true of the -2 contour. Notice the truncation of fractional power at wave number 24 as evidenced by the vertical sections of contour along this wave number. This is a remnant from the truncation of zonal wave number 24 imposed in the Flattery analysis. In comparing the q and W curves with those for the other four quantities, one observes that for v, q, and W, the power is more spread out toward higher wave numbers than is the case with the u, T and Z plots. Again, the -2 contour shows this most clearly. For example, the -2 (1%) contour lies generally along the equatorial wave number 20 curve for q, whereas for T it follows the wave number 16 curve, especially in the Northern Hemisphere. The T and Z curves tend to show a restriction of power to lower wave numbers in mid-latitudes, and more spectral spreading in the tropics. Such a pattern is not evident in the q and W plots, in which the 1% contour generally follows the dashed constant wavelength curves at all latitudes.

Table 3 gives a quantitative comparison of the zonal eddy power distribution by wave number bands at 40°N. At this latitude, the shift of zonal eddy power to higher wave numbers with height for q and W is clearly evident for JAN, but is totally absent in the JUL case. Just the opposite is true for T and Z, in which no power shift with height is evident in the JAN case but is quite pronounced in the JUL case. This same shift is evident to a lesser extent for u. The power distribution for v remains consistent for both cases and levels, with the vast majority of the zonal eddy power lying in the middle band.

TABLE 3. FRACTIONAL CONTRIBUTIONS TO TOTAL EDDY POWER IN ZONAL HARMONICS SPECTRUM FOR 40°N FROM THREE WAVE NUMBER BANDS

DATE	LEVEL	WAVE NUMBER BAND	u	v	T	Z	q	W
JAN	850	1-2	.46	.08	.55	.61	.46	.50
		3-10	.47	.72	.39	.37	.41	.39
		11-20	.06	.17	.05	.02	.11	.09
	500	1-2	.42	.04	.59	.57	.31	.31
		3-10	.52	.77	.35	.41	.52	.53
		11-20	.06	.16	.05	.02	.14	.13
JUL	850	1-2	.36	.13	.63	.71	.25	.31
		3-10	.50	.65	.31	.28	.53	.51
		11-20	.11	.18	.05	.01	.17	.13
	500	1-2	.16	.04	.32	.35	.24	.31
		3-10	.67	.69	.55	.59	.53	.50
		11-20	.15	.24	.11	.06	.19	.15

After the zonal harmonic analysis, each global departure field was expanded in a spherical harmonic expansion of the form

$$A^*(\phi,\lambda) = \sum_{m=0}^{M} \sum_{n=m}^{m+N} [\alpha_n^m \cos m\lambda + \beta_n^m \sin m\lambda] P_n^m (\sin \phi) \qquad (9)$$

where N represents the truncation limit of the quantity n-m, which for the associated Legendre function $P_n^m (\sin \phi)$ represents the number of times the function has a value of zero between the poles. Thus n-m can be thought of as a type of meridional wave number as a counterpart to the zonal wave number m, whose truncation limit is set at M = 32 for this expansion. To evaluate the coefficients α_n^m and β_n^m, the A* values at the grid points were interpolated linearly to the Gaussian latitudes, and a fast Fourier transform was used to evaluate the coefficients γ_{m_k} and δ_{m_k} of the zonal expansion

$$A^* (\phi_k,\lambda) = \sum_{m=0}^{M} \gamma_{m_k} \cos m\lambda + \delta_{m_k} \sin m\lambda \qquad (10)$$

where k represents the indices of the Gaussian latitudes along which this expansion was carried out, and γ_{m_k}, δ_{m_k} are given by

$$\begin{aligned} \gamma_{m_k} &= \sum_{n=m}^{m+N} \alpha_n^m P_n^m (\mu_k) \\ \delta_{m_k} &= \sum_{n=m}^{m+N} \beta_n^m P_n^m (\mu_k) \end{aligned} \qquad (11)$$

where $\mu_k = \sin \phi_k$. Using the orthonormality of P_n^m with values of P_r^m that normalize to unity, we have

$$\begin{aligned} \alpha_n^m &= \int_{-1}^{1} \gamma_{m_k} P_n^m (\mu)\, d\mu \\ \beta_n^m &= \int_{-1}^{1} \delta_{m_k} P_n^m (\mu)\, d\mu. \end{aligned} \qquad (12)$$

These integrals were evaluated using the Gaussian quadrature technique. For M = 32 and 64 Gaussian latitudes, the highest order P_n^m that can be integrated exactly is P_{63}^{32}, so N = 31 was chosen to complete the rhomboidal truncation of the spherical harmonic expansion. Once these numerical integrations were carried out, the weekly averaged spherical power was used to calculate the normalized spherical harmonic power:

$$\Delta_n^m = \frac{\{(\alpha_n^m)^2 + (\beta_n^m)^2\}}{\sum_{m=0}^{M} \sum_{n=m}^{m+N} \{(\alpha_n^m)^2 + (\beta_n^m)^2\}} . \qquad (13)$$

Figs 6a-d display Δ_n^m plotted in $\log_{10}$ form on an n-m vs. m plot. The contour labels are the powers of 10 corresponding to the fractional contributions at each (n-m,m) ordered pair of modes. The sum of the fractional contribution from each ordered pair over the entire plot is unity. Here, the -3 and -5 contours alone are shown for clarity -- they correspond to a 0.1 and 0.001 percent contribution to the total spherical power, respectively. The 24 wave number truncation is somewhat evident in the plots as was the case with the zonal power plots. In these plots, the largest spectral spreading seems to be occurring in the wind components. Both contours on the v diagrams lie at relatively high wave numbers in both directions, while the u curves are spread out in primarily the meridional direction. This is certainly consistent with the plot of the zonally averaged departure of u in Fig. 3 which showed a predominance for several waves from pole to pole. The wind component plots show very little variation with height in comparison with the other four quantities. While the contours on the q and W plots lie at higher wave numbers in both directions at 500 mb than at 850 mb for both months, just the opposite is true for Z and to a lesser degree, T. Also, for any given month and height, it is clear that T and Z have a greater percent of their power in lower wave numbers than do the other four quantities. In general, it appears that T and Z are most restrictive in concentrating power in low wave numbers, q and W are less so, and u and v hold a greater share of their spectral power in higher wave numbers.

These findings are illustrated in another way in Figs. 7a-b. Here cumulative fraction of the power contributed by all of the components that have both n-m and m less than or equal to the value of "wave number" on the abscissa is plotted against wave number. Thus, for example, the value plotted on the figure at wave number 2 represents the sum of the fractional power contributions from all wave number combinations such that both m and n-m are less than or equal to 2. The large jumps on the graphs at "wave number" = 2 show the dominance of the n-m = 2, m = 0 component in the T, Z, q, and W harmonics. While this harmonic is not nearly as dominant at 850 mb as it is at 500 mb for Z, the dominance is nearly the same at both heights for T,

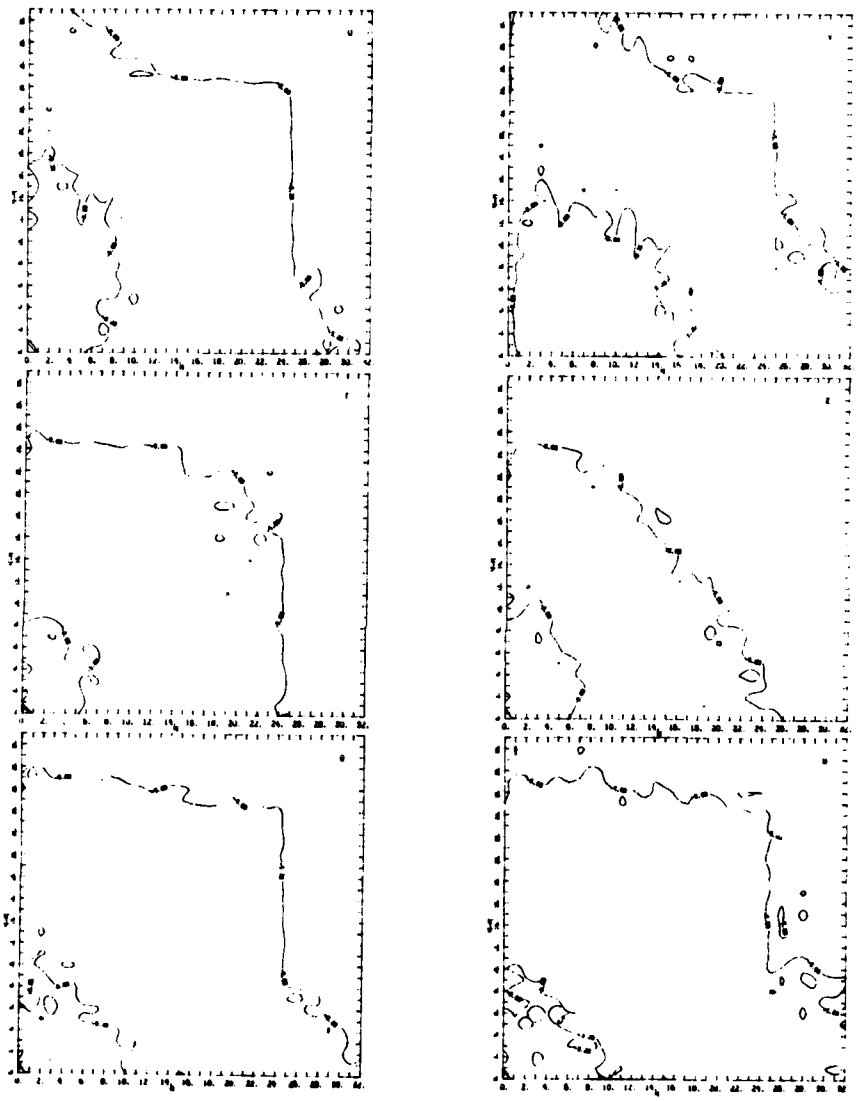

Fig. 6a. Weekly averaged normalized spherical eddy power for JAN at 850 mb. Contour labels are powers of 10 corresponding to the fractional contribution of each wave number (n-m,m) ordered pair. The value n-m is the number of zeros the curve passes through between the poles.

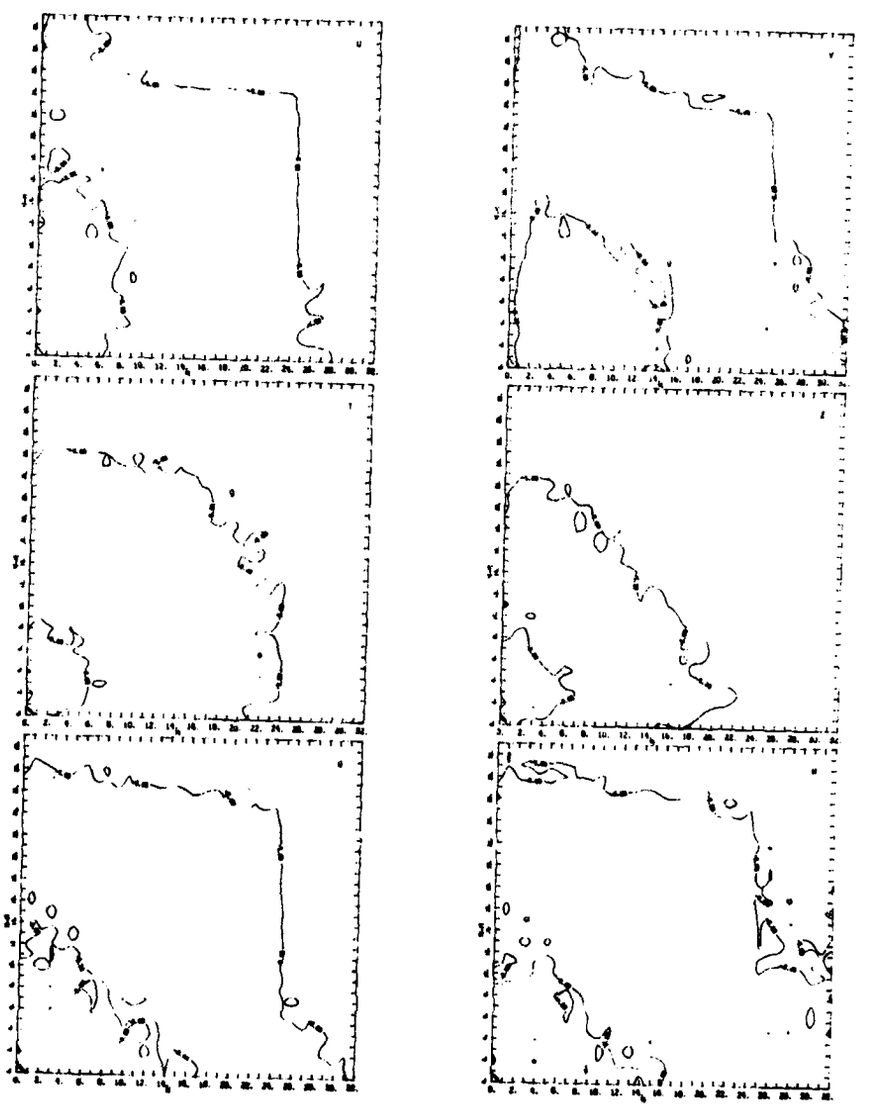

Fig. 6b. Weekly averaged normalized spherical eddy power for JAN at 500 mb.

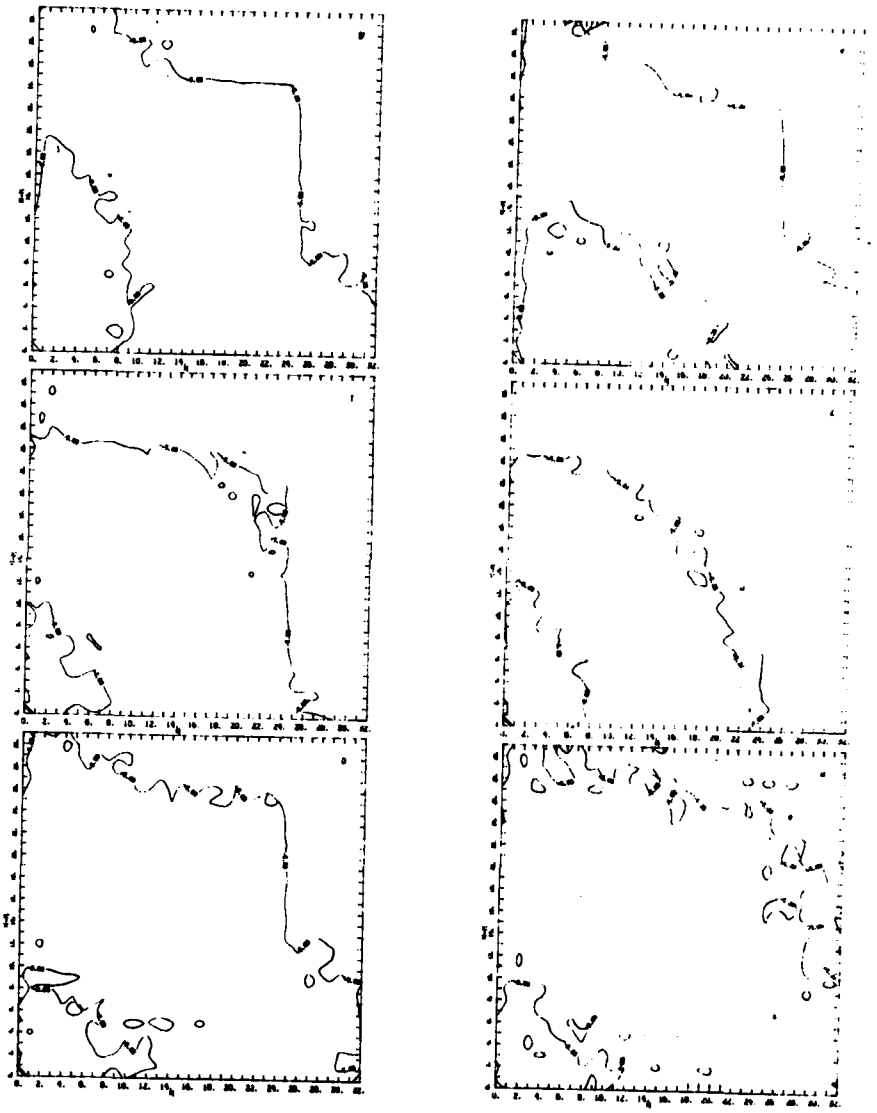

Fig. 6c. Weekly averaged normalized spherical eddy power for JUL at 850 mb.

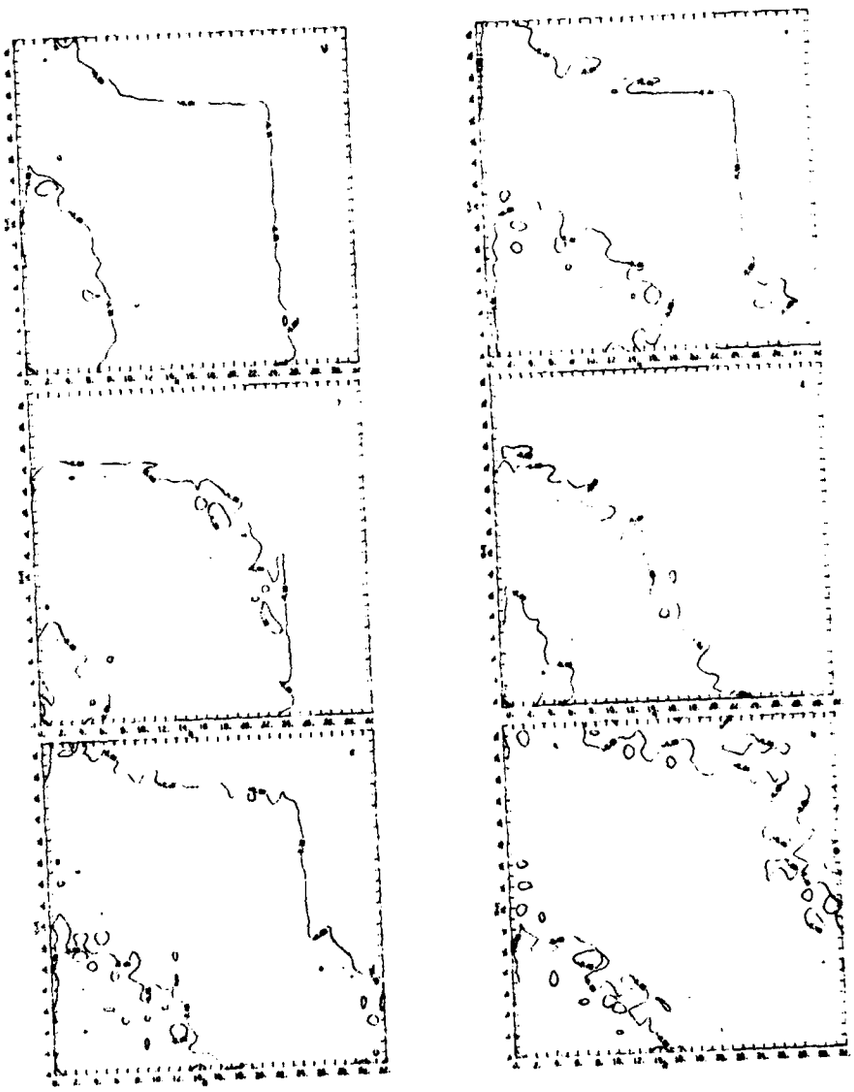

Fig. 6d. Weekly averaged normalized spherical eddy power for JUL at 500 mb.

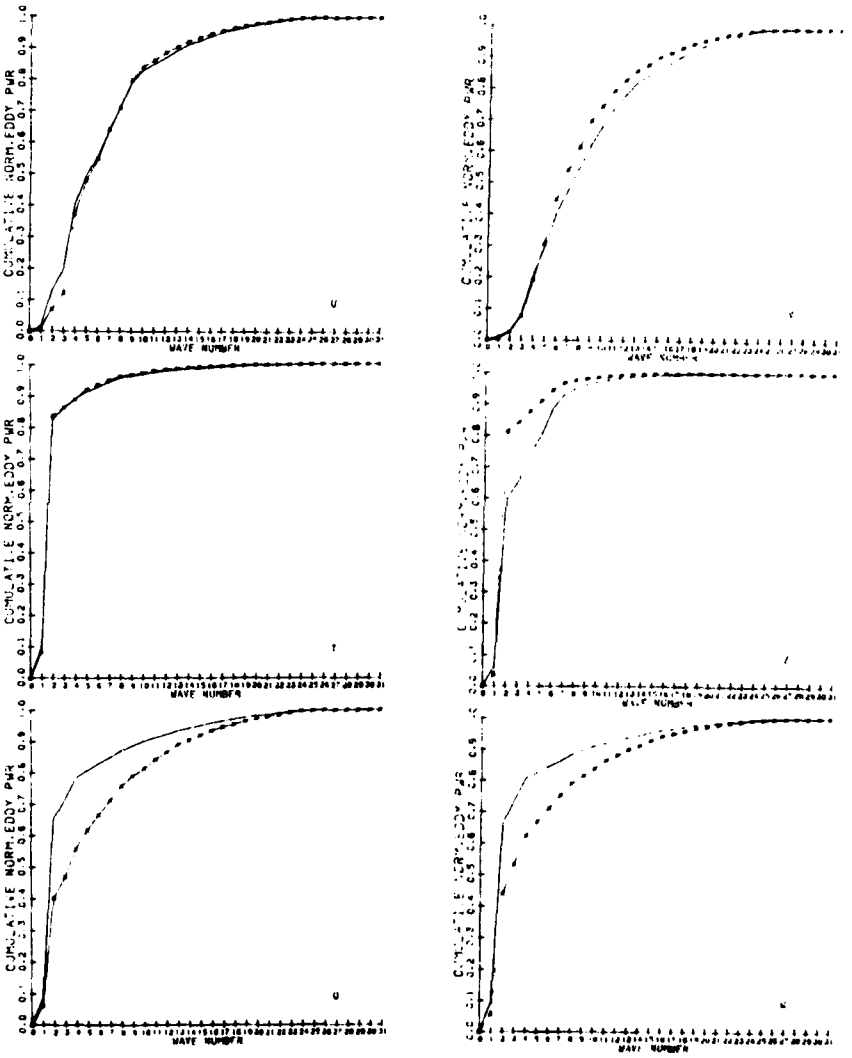

Fig. 7a. Cumulative normalized eddy power for JAN at 850 mb ——— and 500 mb x—x—x. "Wave number" on the abscissa refers to equal values of n-m and m on Figs. 6a-d over which the fractional contributions were summed to produce these plots.

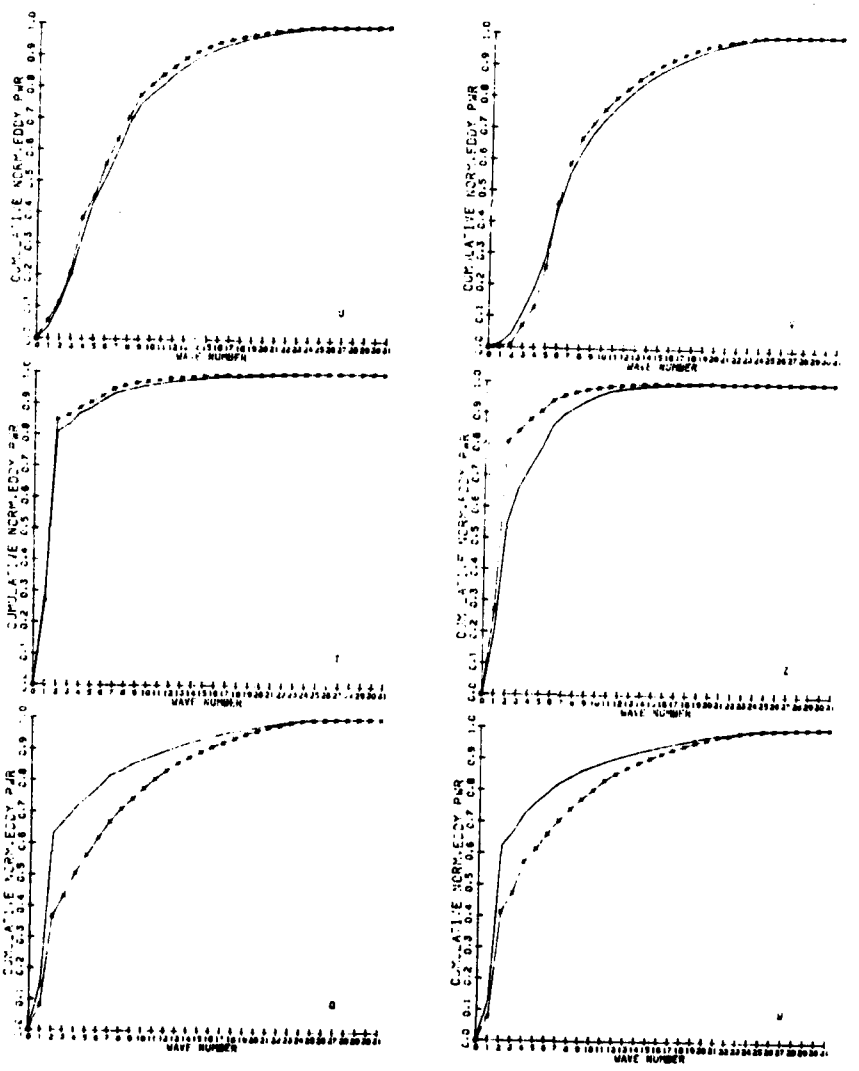

Fig. 7b. Cumulative normalized eddy power for JUL at 850 mb ——— and 500 mb x—x—x.

and the q and W plots reveal a greater dominance in this harmonic at 850 mb. Primarily because of this and the fractional contributions up to about "wave number" 12, a rhomboidal truncation set at 12 in an analysis would clearly include essentially all of the power for T and Z, whereas a significant portion would be missing for q and W, especially at 500 mb. Such a truncation would create an even more serious distortion in an attempt to represent the wind field, since a good share of its power contribution lies in wave numbers greater than 10. This is revealed more quantitatively in Table 4, in which the fractional spherical hormonics contributions from three "wave number" bands are listed.

TABLE 4. CONTRIBUTIONS TO TOTAL EDDY POWER IN SPHERICAL HARMONICS SPECTRUM FROM THREE WAVE NUMBER BANDS

DATE	LEVEL	WAVE NUMBER BAND	u	v	T	Z	q	W
		1-2	.13	.03	.82	.60	.65	.66
	850	3-10	.70	.65	.14	.37	.25	.25
		11-20	.15	.27	.03	.03	.08	.07
JAN								
		1-2	.07	.02	.84	.81	.40	.44
	500	3-10	.77	.72	.14	.17	.41	.40
		11-20	.14	.22	.02	.01	.16	.14
		1-2	.11	.04	.81	.54	.63	.62
	850	3-10	.67	.69	.15	.41	.24	.25
		11-20	.19	.23	.04	.04	.10	.09
JUL								
		1-2	.11	.01	.85	.81	.37	.41
	500	3-10	.70	.75	.12	.17	.41	.39
		11-20	.17	.21	.02	.02	.19	.16

A significant fraction of the power lies in the 11-20 band for u and v. The fraction from this band is less for the moisture quantities, and almost insignificant for T and Z. The table also illustrates the relative constancy of u, v, and T between season and height, and the relative shift of power with height of Z compared to q and W. Finally, it shows that wave number 1-2 contributions for Z are slightly less than for q and W at 850 mb but rise to be equal to T at 500 mb.

The dominant harmonic for T, Z, q, and W is the n-m = 2, m = 0 harmonic which is the zonal mean of each quantity which has a maximum at the equator and minima at the poles. The fractional power contribution from this harmonic is given in Table 5, along with the contribution from the n-m = 1, m = 0 harmonic. The results show that while the n-m = 2 harmonic is clearly the dominant one in all cases, the n-m = 1 (maximum at one pole, minimum at

the other) becomes larger at the expense of the n-m = 2 component in JUL in T and Z. For q and W, the seasonal decrease of the n-m = 2 contribution is not as large, and it is not the n-m = 1 component that appreciably benefits from its decrease. The probable explanation for the greater n-m = 1 contribution in the summer from T and Z is the higher hemispheric summer temperature in one hemisphere over the other. When zonally averaged temperatures for 1/15/78 and 7/20/78 (both at 00GMT, 850 mb) were plotted as a function of latitude, (see Figs. 8a,b) the 1/15/78 case depicted much greater symmetry about the equator than the 7/20/78 plot. The 7/20/78 case clearly shows a combination of both a wave number 1 and 2 component in it (Northern Hemisphere latitude values substantially greater than Southern Hemisphere counterparts, and absolute maximum shifted northward) whereas in the 1/15/78 plot there is no clear dominance of the Southern Hemisphere values over corresponding Northern Hemisphere values. The same was true at 500 mb for both T and Z (not shown). As a direct result of this, there is somewhat less symmetry about the equator in the zonally averaged q values for 7/20/78 than there is for 1/15/78 (see Figs. 8c,d). Since these comparisons are based on only one observation time in each season, the results are not conclusive. However, on the basis of these plots it appears that the summer zonally averaged temperature is higher in the Northern Hemisphere than in the Southern Hemisphere. A larger land to ocean ratio in the Northern Hemisphere is the probable explanation for this, due to greater atmospheric heating over land.

TABLE 5. FRACTIONAL CONTRIBUTION FROM THE ZONAL AVERAGE, MERIDIONAL WAVE NUMBER 1 AND 2 HARMONICS

DATE	LEVEL	n-m	T	Z	q	W
JAN	850	1	.08	.01	.05	.05
		2	.67	.50	.54	.54
	500	1	.07	.01	.04	.04
		2	.73	.76	.31	.36
JUL	850	1	.25	.13	.09	.08
		2	.50	.26	.44	.44
	500	1	.26	.27	.03	.03
		2	.57	.53	.25	.28

The values for weekly averaged total power, the denominator in the expression for Δ_n^m, are given in Table 6. Because the values are dimensional and because of the normal variation with height expected in each variable, a comparison of variation in season only can be made between the variables.

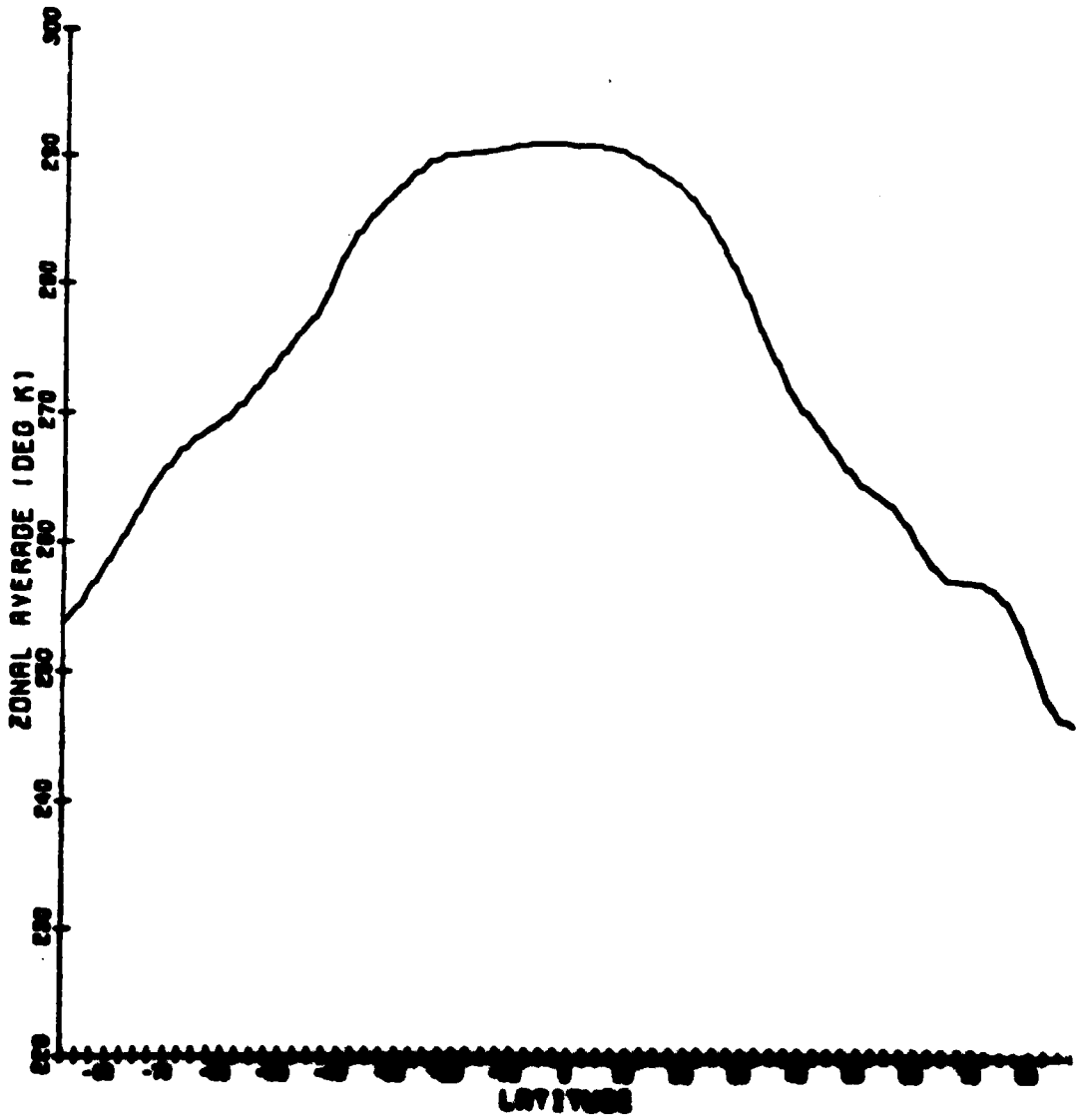

Fig. 8a. Zonally averaged temperature for 1/15/78 00GMT at 850 mb, computed from corrected field.

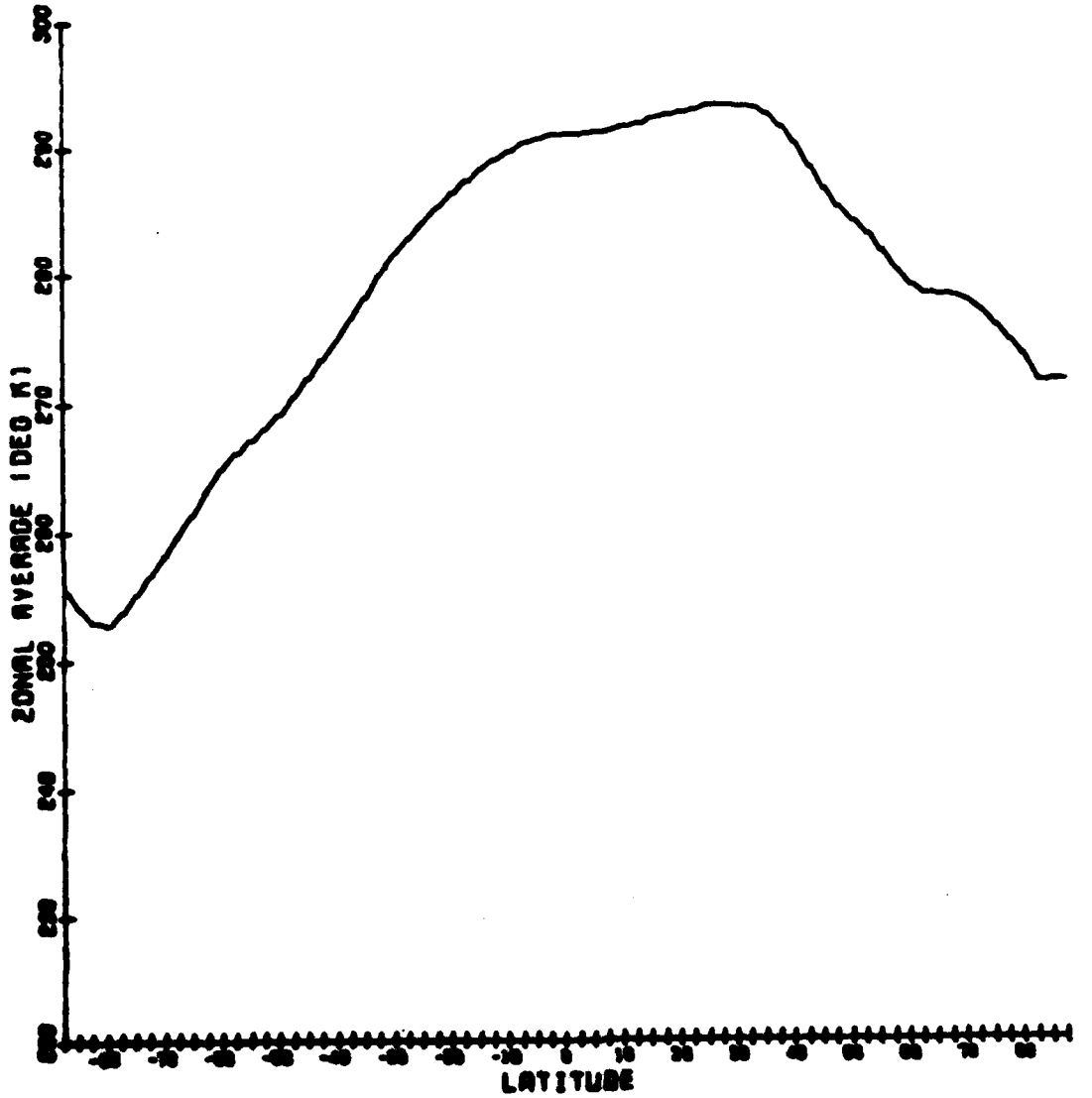

Fig. 8b. Zonally averaged temperature for 7/20/78 00GMT at 850 mb, computed from corrected field.

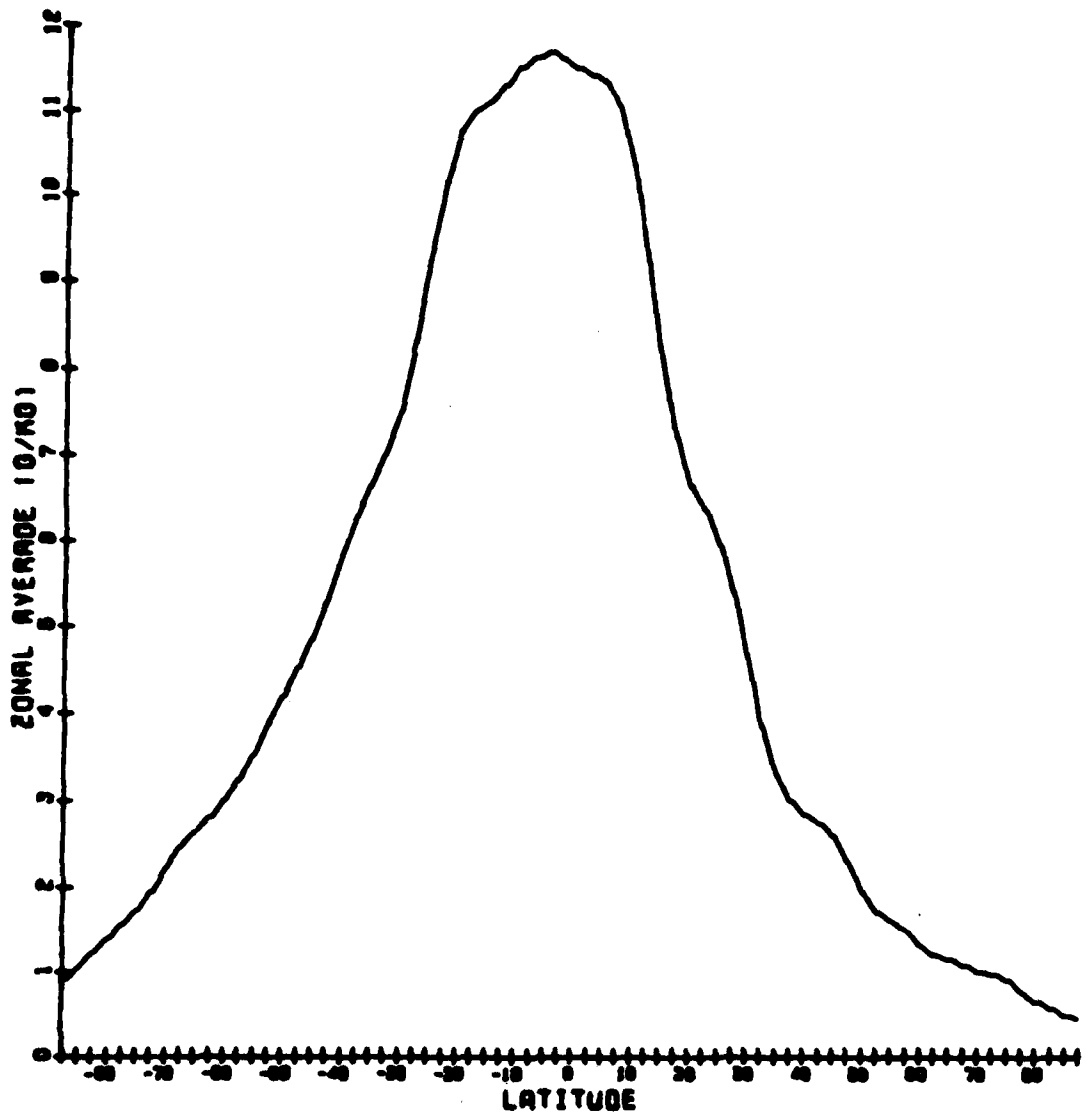

Fig. 8c. Zonally averaged specific humidity for 1/15/78 00GMT at 850 mb, computed for corrected field.

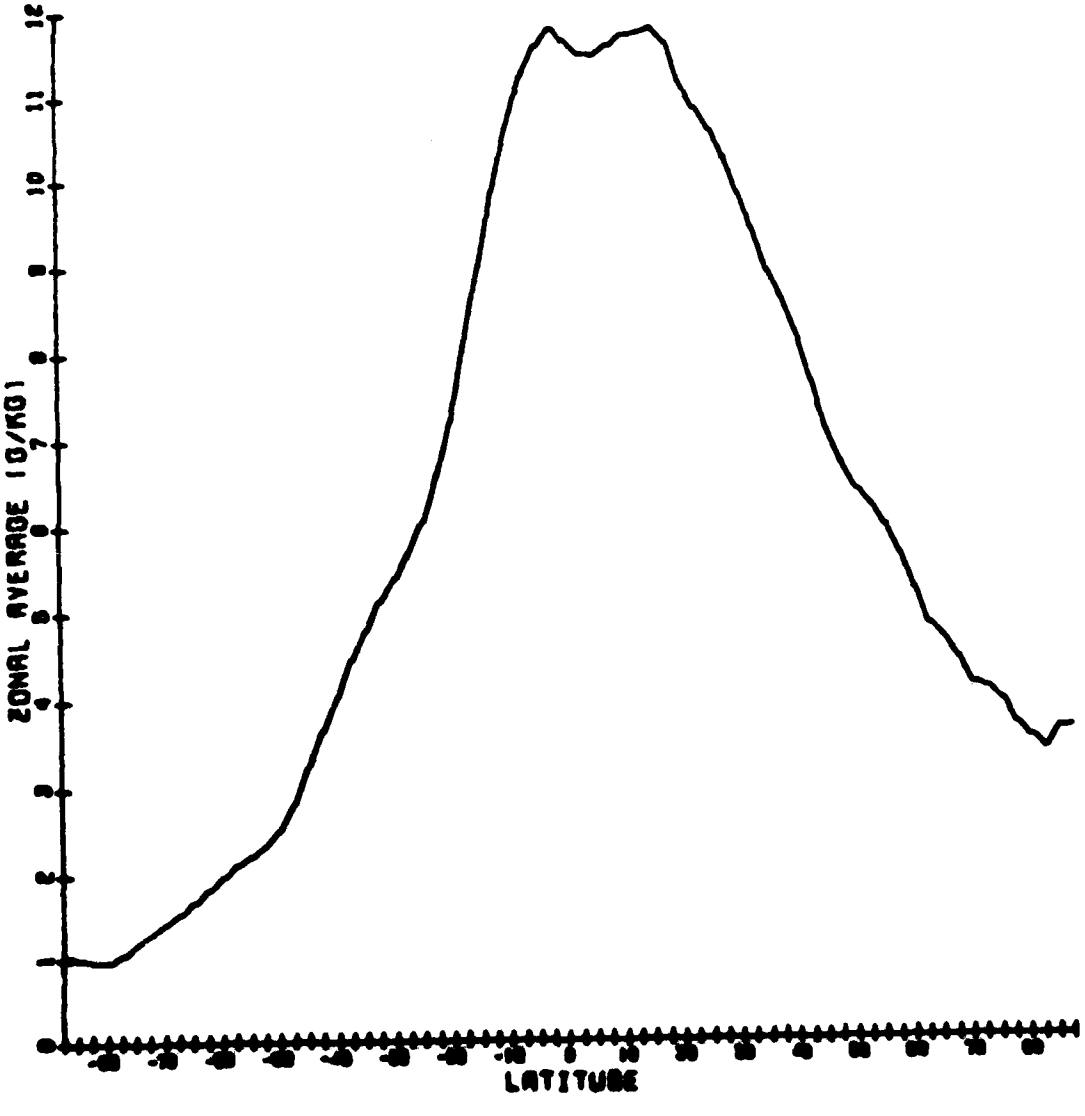

Fig. 8d. Zonally averaged specific humidity for 7/20/78 00GMT at 850 mb, computed from corrected field.

With the exception of v at 850 mb, all of the quantities except q and W show a decrease in total power from JAN to JUL. The zonal eddy power was greater in the winter hemisphere, and it is likely that the larger number of observations in the Northern Hemisphere resulted in a somewhat more irregular corrected field in data rich areas compared to the smoother corrected field in data sparse areas, contributing to the larger power. The lower zonal eddy power for the moisture variables in the winter hemisphere (see Fig. 3) is probably offset by the greater variation (due to greater data density) in the Northern Hemisphere moisture fields compared to that of the Southern Hemisphere, resulting in very little variation in total power with season.

TABLE 6. TOTAL POWER FOR SPHERICAL HARMONICS

		$u\ (m/s)^2$	$v\ (m/s)^2$	$T\ (^oK)^2$	$Z\ (gpm)^2$	$q\ (g/kg)^2$	$W\ (cm)^2$
JAN	850	200.7	100.6	349.0	38103.4	45.1	4.6
JAN	500	498.1	250.5	297.1	179664.2	6.7	1.0
JUL	850	167.8	103.5	251.9	23104.6	43.0	4.1
JUL	500	353.4	202.1	226.9	120152.9	5.8	0.9

IV. Impact of Results on Objective Analysis Methods for Moisture

It is evident that the observed moisture field has certain spectral characteristics that make it uniquely different from the motion and mass fields. In the preparation of initial conditions for a numerical weather prediction model, any gridded representation of the moisture field should possess these same spectral characteristics in order to provide an accurate initial condition for a global model. In fact, these characteristics can also be used to assess the accuracy of the model output results as well. As mentioned in the beginning of this report, the importance of analysis accuracy in the model forecast will depend on the model itself. However, the more faithful the model is to the simulation of natural processes, the more it will depend on realistic initial conditions to generate good forecasts, especially for short-term forecasts. With all of the present emphasis on forecast model improvement, it is certainly timely to focus attention on accuracy in the production of model initial conditions.

Within the spectral range that can be accurately resolved by the rawinsonde network, the spectral results of this study are an accurate representation of the spectral characteristics of the global moisture distribution. They therefore can be used as a standard, especially in the lower (less than, say, wave number 20) waves, against which the representations from any analy-

sis scheme should be tested for their accuracy. The zonal and spherical harmonic analyses of the gridded fields produced by the analysis scheme should demonstrate the same relative features as those that are shown in this study. Any major differences would point to particular problems that may exist in the analysis scheme and its ability to represent the fields spectrally.

The faithfulness of analysis schemes in the spectral representation of the observed field may or may not be influenced by the "closeness of fit" of the gridded values to the observations. For example, if the amplitudes of the spectral components were in good agreement with those of the observations but the two fields were out of phase, the analysis would test out well spectrally but would be a failure in physical space. Both a "closeness of fit" in physical space and a harmonic analysis in spectral space must be performed to determine if the analyzed field is a suitable representation of the observations. Both tests were conducted in this study using the Flattery analysis as the test analysis scheme. To test for closeness of fit in physical space, the quantity

$$\left[\frac{1}{N}\sum_{i=1}^{N}(F_i^* - OB_i^*)^2\right]^{\frac{1}{2}} \Bigg/ \left[\frac{1}{N}\sum_{i=1}^{N}(OB_i^*)^2\right]^{\frac{1}{2}} \qquad (14)$$

was calculated using the Flattery values (F) and observations (OB) for 1/15/78 00GMT and 7/16/78 00GMT. The Flattery analysis values were interpolated bilinearly to the observation sites, their global mean was removed, and they were compared with the departures of the N observed values (departures from the Flattery global mean, found to be very close to global mean calculated from corrected fields) for u, v, T, Z, and q. The smaller the value of this quantity, the better the overall fit of the analysis field to the observations. Table 7 lists the results of these calculations. The values for T and Z are generally the best, except for Z, 1/15/78, at 850 mb. The accuracy of the analysis of u and v seems to improve with height, but in all cases it is not as good as the accuracy of T and Z. The accuracy of the analysis of q seems to be more seasonal than the rest of the quantities, with accuracy decreasing from winter to summer by about the same amount at both levels. It appears on the basis of these tests that q is a little more accurately analyzed than are u and v, but less accurately than T and Z.

TABLE 7. NORMALIZED RMS ERROR OF FLATTERY ANALYSIS

		1/15/78	7/16/78
850	u	.51	.59
	v	.54	.76
	T	.18	.23
	Z	.36	.16
	q	.30	.55
500	u	.31	.37
	v	.34	.33
	T	.13	.20
	Z	.09	.13
	q	.30	.58

A direct spectral comparison of the Flattery analyses with the observations is not possible due to the spatial irregularity of the observations. The best that can be done is a comparison of the Flattery power spectra with those of the corrected fields, which was suggested earlier as a basis for spectral accuracy of the analysis. Such a comparison is given for the January weekly averages in Figs. 9a,b. The solid curves are the base 10 logarithm of the fractional spherical harmonic power for the Flattery fields, while the dashed curves are a reproduction of the curves for the corrected fields from Fig. 6. Except for larger contributions to the total power from higher wave numbers, the figures do not show very much difference in spectral configuration between the Flattery and corrected fields. In fact, except for the case of Z, and to a lesser extent T, it appears that the change brought about by the corrections consisted primarily in adding back in the high wave number variation that was removed in the wave number 24 truncation of the Flattery analysis. This suggests that, spectrally, the major difference between the two fields is in the amplitudes of the shortest waves. The total power was not changed significantly by the corrections, either. For the weekly averaged January values, the total power increased from 1 percent for T at 500 mb to 12 percent for v at 850 mb. Thus, the apportionment of power among the wave numbers and the total spherical power are very close to the same in both fields.

In this case, there is favorable spectral agreement between the corrected fields and Flattery analysis fields, but according to Table 7 there are appreciable errors when the Flattery fields are compared to the observations. This apparent discrepancy could be explained in one of two ways: (a) the amplitudes of the two fields are similar, but they are out of phase with each other, or (b) the corrected fields are more like the Flattery

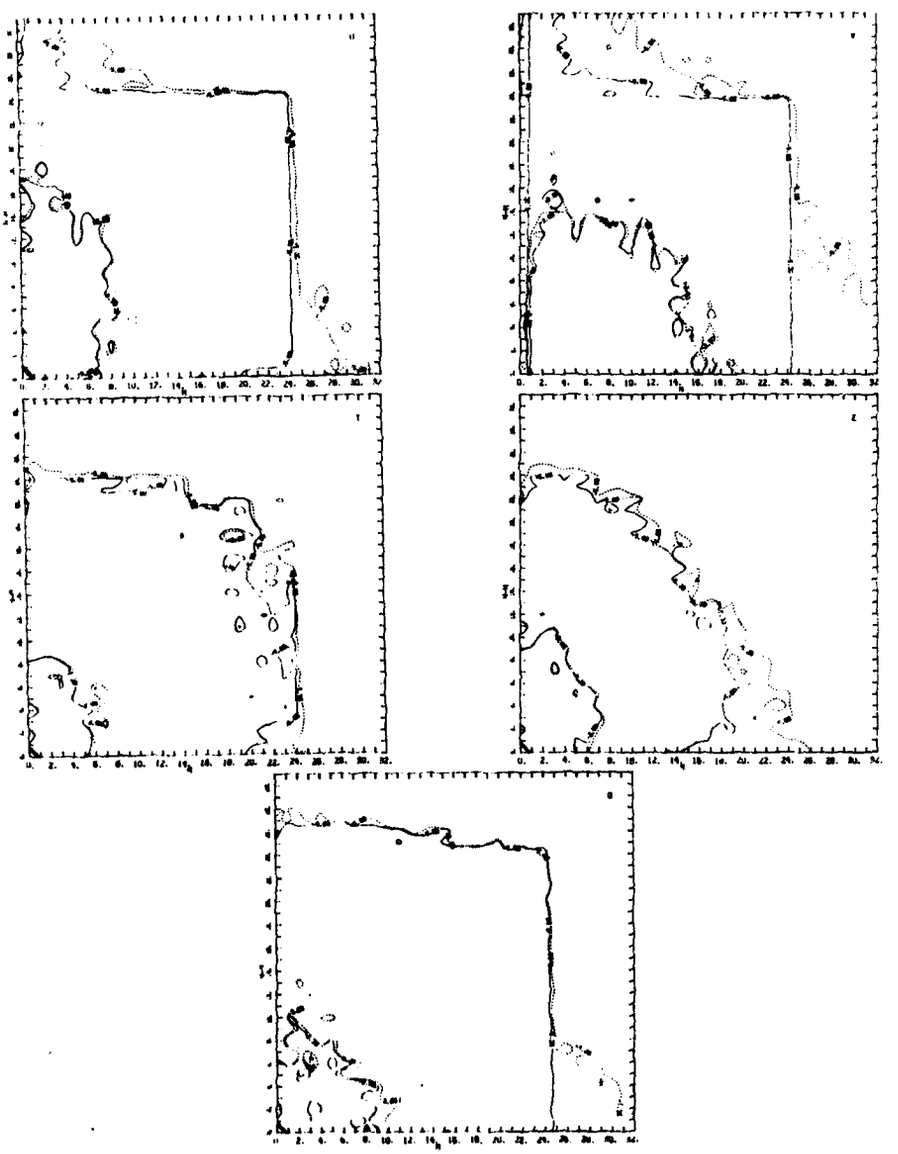

Fig. 9a. Weekly averaged normalized spherical eddy power for JAN at 850 mb. Solid contours represent Flattery analysis values, dashed contours represent corrected field values (identical to Fig. 6).

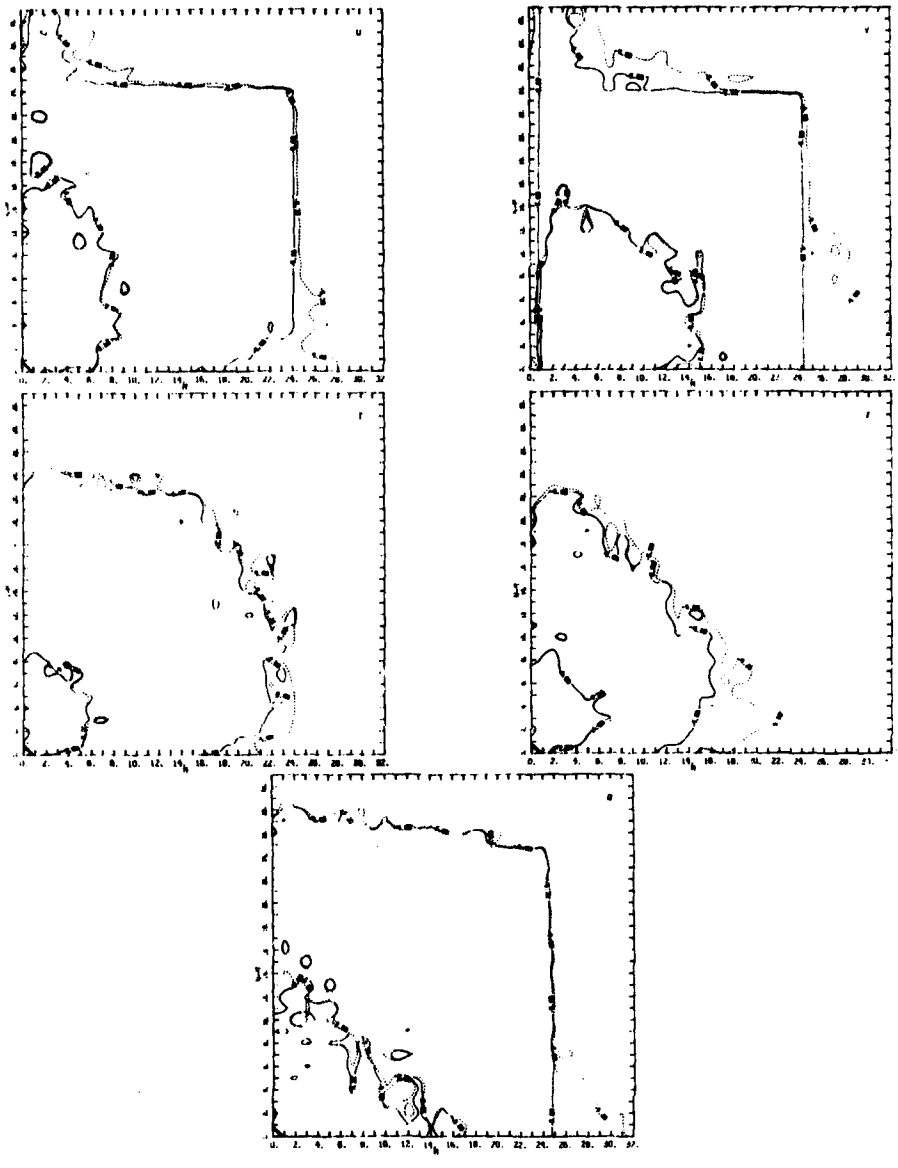

Fig. 9b. Weekly averaged normalized spherical eddy power for JAN at 500 mb. Solid contours represent Flattery analysis values, dashed contours represent corrected field values (identical to Fig. 6).

analysis fields than they are like the observations, so that comparing the Flattery analyses with the corrected fields is not like comparing them with the observations. Looking back at Table 1, there is certainly some evidence that most of the corrected fields have only been brought less than half way towards the observations from the Flattery analyses. Thus, they are for the most part more a product of the Flattery analysis than they are of the observations. However, in order to examine the possibility of a phase error, the absolute value of the error between the corrected fields and the Flattery analyses must be computed. Values for the globally averaged absolute value of the difference between the two fields are given in Table 8, along with the differences between the global averages of corrected fields and Flattery fields. The units for the quantities in the first two columns are given, and the values in parentheses are the ratio of the magnitude of the values in the second column to those in the first. Note that the absolute error between the two fields is small compared to the average magnitude of each quantity (column 4) especially for T, Z, and q, so that a relatively small phase shift occurs in the corrected field with respect to the Flattery field. However, notice that the bias ([C] - [F]) values, though they are small in magnitude, make up a significant fraction of the total magnitude difference (column 1) between the fields for those quantities (T, Z, and q) which showed the most significant amount of correction as seen in Table 1. It is concluded from these results that changes in the Flattery fields due to the successive corrections were relatively small, but were appreciably effective in biasing the fields towards the observations, especially for T, Z, and q.

TABLE 8. GLOBAL AVERAGE OF DIFFERENCES BETWEEN CORRECTED AND FLATTERY FIELDS FOR JANUARY WEEK

		$[\lvert C_i - F_i \rvert]$	$[C] - [F]$	$\frac{[C] - [F]}{[\lvert C_i - F_i \rvert]}$	$\frac{[\lvert C_i - F_i \rvert]}{[\lvert F \rvert]}$
850	u	.909 ms^{-1}	-.165	(.18)	.141
	v	.855 ms^{-1}	-.036	(.04)	.242
	T	.537 ^{o}K	-.247	(.46)	.002
	Z	4.192 gpm	.707	(.17)	.003
	q	.387 g kg^{-1}	-.202	(.52)	.056
500	u	.924	-.006	(.01)	.084
	v	.896	.040	(.05)	.104
	T	.315	-.166	(.53)	.001
	Z	6.223	2.532	(.41)	.001
	q	.118	-.044	(.38)	.065

In summarizing the comparison between the Flattery fields and the corrected fields, it is evident that the corrected fields still have many of the physical and spectral characteristics of the Flattery fields. Both the absolute difference averaged over grid points and the difference in apportionment of power were small between the two fields for all of the quantities. That the phase error is small is a tribute to the Flattery scheme in that highs and lows and minima and maxima had the same locations as indicated by the observations. Furthermore, the relative amplitudes of the waves were generally preserved by the analysis. The corrections acted in such a way as to draw the average value of the field more toward that of the observations (especially for T, Z, and q) rather than change the fields at particular locations.

V. Summary and Conclusions

The following is a summary of the similarities and differences noted when comparing the spectral characteristics of global specific humidity and layer precipitable water fields with those of zonal and meridional wind components, temperature, and geopotential height:

a. The variation of the zonal mean power of T, Z, q, W with latitude is similar for all four quantities, with a maximum at the equator and a minimum at the poles. The zonal mean for q and W is equal to the global mean at latitudes lower than for T and Z, indicating a larger meridional gradient of the zonal mean for the moisture quantities. The latitudinal variation of the zonal mean of u reflects the distribution of easterlies and westerlies and thus oscillates several times between the poles.

b. The latitudinal distribution of total zonal eddy power reveals a bimodal character for T and Z, with maxima at mid-latitudes and minima at the equator and both poles. This is also true for u and v, although to a somewhat less pronounced extent. The moisture variables have a zonal eddy power which is a broad maximum at equatorial latitudes and a minimum at both poles. It appears that this latitudinal structure is primarily due to the saturation specific humidity acting as a more severe limit to the variation about the zonal mean in colder regions than it is in warmer regions because of its lower value at lower temperatures.

c. The zonal harmonic analysis results showed that the power was more restricted to lower wave numbers for u, T, and Z, and more spectral spreading

was evident in v, q, and W. The T and Z spectral distribution varied more significantly with latitude, with a greater restriction of power to lower wave numbers at mid-latitudes and more spectral spreading in the tropics. Power shifts to lower wave numbers with height were evident in the January case for q and W and in the July case for T and Z.

d. In the spherical harmonic results, the wind components show the greatest spectral spreading, with most of their power in the composite wave number 3-10 band. They also have a significant amount of their power in the 11-20 wave number band. This is unlike the power distribution for the other four variables, which have a much smaller amount of power (less than 10 percent) contributed by wave numbers greater than 10. There is very little variation in power distribution with height in u and v. The q and W spectra, on the other hand, show power spreading to higher wave numbers with height, while power is more concentrated at lower wave numbers with height for Z and to a lesser extent for T. The power for T results primarily from the number 2 meridional wave of the zonal mean, and there is very little change in this with season or height. In general, T and Z have most of the power in the lowest wave numbers (0-2), q and W have roughly an equal amount of power contributed from low and medium (3-10) wave numbers, and u and v have most of their power from the medium wave numbers, with a significant contribution from the high (11-20) wave numbers.

e. While the meridional wave number 2 component of the zonal mean is the dominant spherical component for T, Z, q, and W, the results showed that the meridional wave number 1 component of the zonal mean grew at the expense of wave number 2 in the July case for T and Z. Thus, the zonal mean values in the Northern Hemisphere in July were higher than their counterparts in the Southern Hemisphere in January, making the July zonal mean temperature plot much more asymmetric about the equator than the January plot. The higher Northern Hemisphere summer temperatures were attributed to the larger land to ocean ratio in that hemisphere. This asymmetry lowered the meridional wave number 2 contribution from q and W as well.

The results presented in this study, to the extent that they are considered an accurate portrayal of the spectral characteristics of the global moisture distribution, are intended to be used as a baseline for testing the reliability of an objective analysis scheme for moisture. Clearly, the unique characteristics of moisture must be faithfully reproduced in the

gridded analysis field, and not be distorted by the analysis method itself. This implies the need for modification of a mass-motion objective analysis scheme to make it useful for moisture analysis, or development of an entirely separate scheme for moisture analysis.


DATE
ILME